論文 / 著書情報
Article / Book Information

題目(和文)	
Title(English)	Nonthermal Plasma-assisted CO2 Conversion Enabling Auto-methanation
著者(和文)	ZHANChunyuan
Author(English)	Chunyuan Zhan
出典(和文)	学位:博士(工学), 学位授与機関:東京工業大学, 報告番号:甲第12533号, 授与年月日:2023年9月22日, 学位の種別:課程博士, 審査員:野﨑 智洋,平田 敦,齊藤 卓志,赤坂 大樹,山本 貴富喜
Citation(English)	Degree:Doctor (Engineering), Conferring organization: Tokyo Institute of Technology, Report number:甲第12533号, Conferred date:2023/9/22, Degree Type:Course doctor, Examiner:,,,,
学位種別(和文)	博士論文
Type(English)	Doctoral Thesis

Doctoral Thesis

Nonthermal Plasma-assisted CO_2 Conversion Enabling Auto-methanation

Chunyuan Zhan

Supervisor:

Professor Tomohiro Nozaki

August 2023

Abstract

In plasma-enhanced CO_2 methanation reaction, as nonthermal plasma (NTP) can provide both heat and radical effect, auto-methanation under NTP treatment becomes possible. This thesis aims to demonstrate the feasibility of the above process on Ru based catalysts. To this end, plasma-enhanced catalytic performance in the packed-bed dielectric barrier discharge (PB-DBD) reactor was confirmed at first. *In situ* diffuse reflectance infrared Fourier-transform spectroscopy (DRIFTS) study indicates carbonate species formation which is enhanced clearly by DBD and its following conversion to CH_4 due to hydrogen spillover on Ru are the key reaction pathways. Auto-methanation was achieved when discharge power was sufficient for reactor to reach the initial reaction temperature. DBD plays important roles as 'ignition' and 'acceleration' once highly reactive species can well interact with catalyst surface.

Nomenclature

CCS	CO_2 capture and storage
CCU	Carbon capture and utilization
DBD	Dielectric barrier discharge
DRIFTS	Diffuse reflectance infrared Fourier-transform spectroscopy
EDS	Energy dispersive X-ray spectroscopy
HAADF-STEM	High-angle annular dark field scanning transmission electron microscopy
LTE	Local thermodynamic equilibrium
non-LTE	non-local thermodynamic equilibrium
NTP	Nonthermal plasma
PB-DBD	Packed-bed dielectric barrier discharge
PtC	*Power-to-Chemicals*
PtM	*Power-to-Methane*
QMS	Quadruple mass spectrometer
SEI	Specific energy input
WHSV	Weight hourly space velocity
XRF	X-ray fluorescence

Table of content

Chapter 1: Introduction

1.1 Overview

With the increase of population and the development of computer science as well as artificial intelligence, the demand for energy is gradually increasing day by day [1,2]. Then energy production becomes important, which is highly related to the issue of global warming. The ever-increasing emissions of CO_2, considered as the major cause of global warming, have increasingly aroused worldwide concern [3-5]. Solutions proposed to this problem are twofold: to reduce CO_2 emissions by CO_2 capture and storage (CCS) as well as to convert exhausted CO_2 into useful fuels and chemicals, known as carbon capture and utilization (CCU) [6-8].

CCS is a technology that recycles CO_2 emitted by factories and power plants, followed by storing these CO_2 gases deep underground [9]. It is indispensable for decarbonization and plays an important role in achieving carbon neutral society. However, it is significant to overcome many technical and economic barriers that exist in this technology before its large-scale deployment. One of them is that it requires a large amount of investment due to its non-profit character [10]. For example, in some countries such as UK and Singapore, CCS is not a feasible option because their geological storage capacity is limited so that it can only be used offshore. This results in high cost in transportation and injection [10].

With increase of high energy demand, recently CCU has attracted much more attention. Compared to CCS, one advantage CCU has is making profits becomes possible as the products obtained from this technology can be sold to the market [10]. Besides, CO_2 is a low-cost and non-toxic resource, more importantly, it will accompany with us all the time compared to the traditional fossil fuels [11]. Although it is energy intensive to convert CO_2 into various products due to its thermodynamic stability, it can be possible that CCU will be widely used because it provides not only the safe supply of chemicals and fuels, but also a competitive price with fossil fuels [11].

Methane, as one of the products that can be obtained by CCU, is one significant

energy carrier to the industry and transportation. It can be used in well-established natural gas infrastructure to heat homes, provide energy for the vehicles or even stabilize the electric power grid [12] [13]. And this helps make one important part of modern economies. The debate about the limitation of fossil fuels and climate change has led to an increase in research expenditure related to methanation in the past few years [14]. Biological methanation is carried out in stirred tank reactors or trickle-bed reactors at temperatures less than 70 °C [12] [15] [16]. In comparison, to reach acceptable methane yield, catalytic methanation is mainly carried out in fixed-bed reactors at temperatures above 250 °C [17] [18]. There are 2 types of methanation processes that have been studied. For one, CO methanation is used to produce natural gas substitutes with coal or biomass gasification [19]. For another, CO_2 methanation is used for electricity storage and prevention of climate change [14] [20]. In this study, CO_2 methanation was investigated as reducing CO_2 emissions is one of our targets.

1.2 CO_2 methanation

1.2.1 Introduction

CO_2 methanation, also known as Sabatier reaction, is an exothermic reaction which follows equation R1.1. It has been first mentioned by Brodie in 1872 and further developed by the French chemists Paul Sabatier and Jean-Baptiste Senderens in 1902 [21-24]. Nowadays, this reaction has attracted people's attention once again because of three aspects including environmental protection, the storage of electrical energy from renewable sources and the space exploration missions.

$$CO_2 + 4H_2 = CH_4 + 2H_2O \quad \Delta H_f^\circ = -165 \text{ kJ/mol} \qquad \text{(R1.1)}$$

CO_2 methanation is one *Power-to-Methane* (PtM) process which can be very suitable for long-term and large-capacity energy storage because it has advantages in discharge time and storage capacity compared to other energy storage technologies [25-

[27]. The details of storage capacity and discharge time comparison are described in Figure 1.1. The PtM can be divided into 3 steps: renewable electricity generation, renewable H_2 production by water electrolysis with utilization of renewable electricity and renewable methane generation by captured CO_2 reacting with renewable H_2.

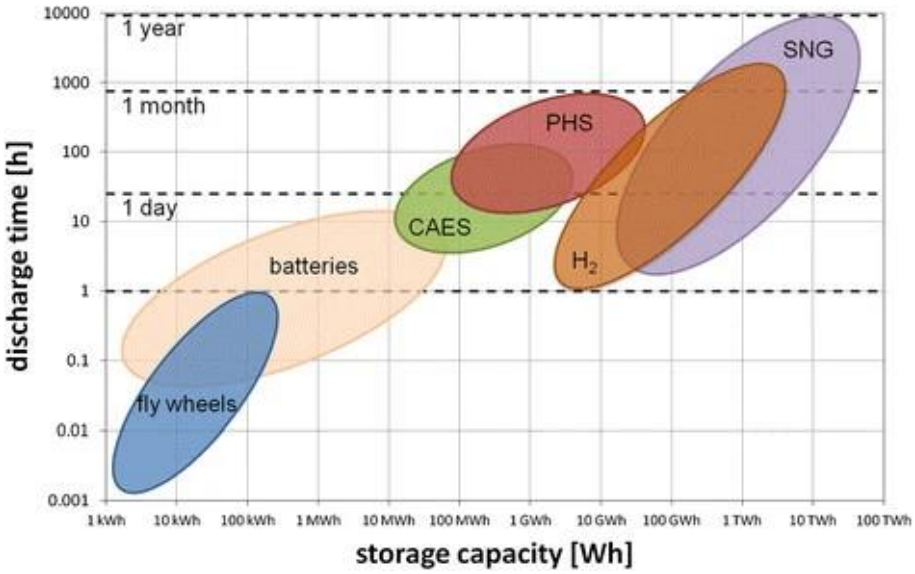

Figure 1.1 Charge/discharge period and storage capacity of different electricity storage systems. (CAES: compressed air energy storage; PHS: pumped hydro storage; SNG: substitute natural gas) [27].

Some PtM facilities have already exist or are currently under construction at the pilot scale [28]. One famous commercial plant, named the Werlte e-gas plant, is the world's first industrially operated plant for catalytic methanation. It produces methane from captured CO_2 in biogas produced by amine scrubbing and H_2 produced by three wind energy alkaline electrolyzers. The key component, methanator, is composed of a long series of tube reactors in which nickel based catalysts are loaded. These reactors are cooled by molten salt and the exchanged heat is used for regeneration of amine scrubbers. This makes the working efficiency of methanator close to about 72 % [12].

Recently, CO_2 methanation is also considered one promising way for long-term space exploration because liquid methane will be utilized instead of hydrogen and kerosene for the sake of long-term usage. Besides, methane is also one good energy

carrier. Compared to hydrogen, it does not lead to metal embrittlement and the bulky highly insulated cryogenic tanks are not necessary [29]. Compared to kerosene, methane is lighter and does not result in coking. More importantly, methane can be obtained by CO_2 methanation in a CO_2-rich environment such as Mars [29].

From thermodynamic perspective, CO_2 methanation favors high pressure and the temperature at which water-gas-shift reaction is little. Figure 1.2 shows thermodynamic equilibrium for the reaction calculated by Gibbs free energy minimization method [30]. At atmospheric pressure, to achieve CO_2 conversion higher than 90 % and methane selectivity close to 100 % simultaneously, reaction temperature should be kept lower than 300 °C. As reaction pressure increases, to achieve the same goal, the feasible temperature region enlarges. In real methane production, H_2/CO_2 ratio should not be lower than 4 because lower ratios cause significant carbon formation which needs to be avoided [31]. In summary, a careful heat management is required to overcome the activation barrier and maintain a favorable gas composition at the same time. Other thermodynamic studies on CO_2 methanation can be found in literature [32-34].

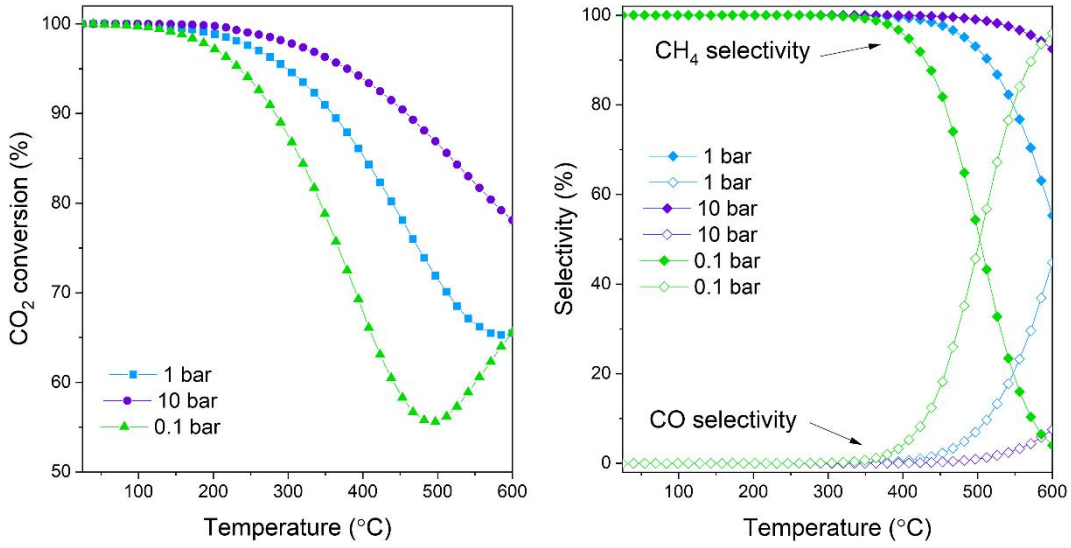

Figure 1.2 Equilibrium of CO_2 conversion, CO and CH_4 selectivity as a function of temperature at different pressures ($H_2/CO_2 = 4$) [30].

1.2.2 Mechanism

Many studies have been carried out to illustrate CO_2 methanation mechanism [35-37]. In summary, some researchers concluded reaction pathway in 3 types [38]. The first is carbide pathway, in which CO is formed through CO_2 dissociation. The second is formate pathway, in which formate is formed as intermediate species. The third is carboxyl pathway, in which carbonhydroxyl is regarded as intermediate species. However, based on literature [39-41], these three pathways can be explained by 2 categories including CO_2 associative route and CO_2 dissociative route [42]. The detailed description on these two schemes is shown in Figure 1.3.

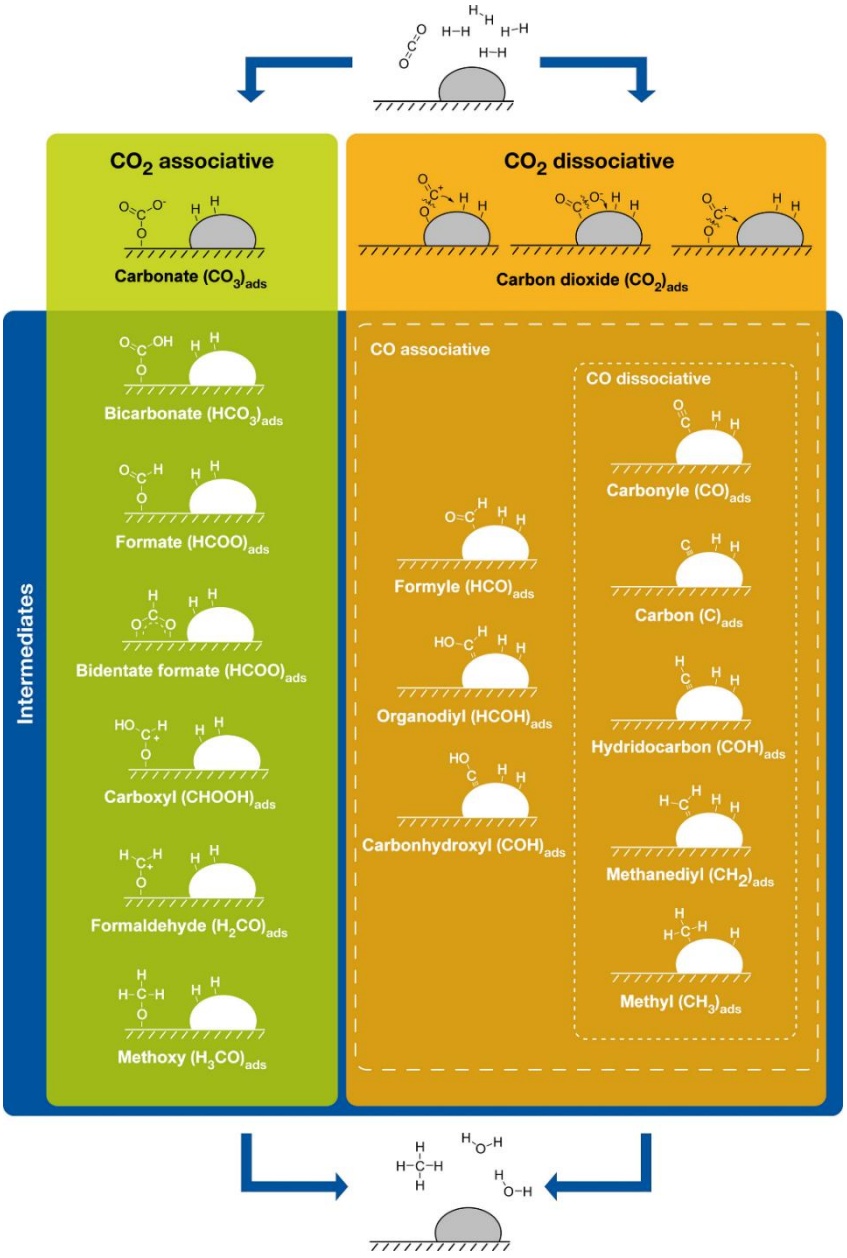

Figure 1.3 The associative and dissociative routes in CO_2 methanation [42].

In CO_2 associative route, CO_2 adsorbs as important intermediate species of carbonate and then reacts with adsorbed H_2 to form several oxygenates such as bicarbonate, formate and formyl. Among these three oxygenates, the formate species is mostly seen in other people's work. Following this pathway, methane can be observed after formaldehyde and methoxy species are generated. One unique feature of this scheme is that no CO can be found [43].

In CO_2 dissociative route, CO_2 dissociates into carbonyl and an oxygen atom at first because C-O bond breaking barrier is reduced at active sites such as step and kink sites [44-47]. Then the reaction follows CO methanation mechanism which can be classified into two categories including CO associative route and CO dissociative route. In CO associative route, intermediate species such as formyl, organodiyl and carbonhydroxyl are generated after CO and H_2 adsorption. Then C-O bond breaks, followed by hydrogenation on the remaining carbon to form the final product of methane. In CO dissociative route, as CO and H_2 adsorb, CO directly converts to the surface carbon and then follows the hydrogenation process.

1.2.3 Challenges

It has been reported that nickel-based catalyst with alumina as support is efficient and active in CO_2 methanation, making its large-scale application possible. However, deactivation of the catalyst is regarded as one big problem which can be caused by poisoning [48], sintering [49], fouling [50] and mechanical straining [51]. There are two ways used to improve both catalytic activity and stability of Ni-based catalyst in CO_2 methanation system. For one, changing the nature of alumina support by hydrotalcite-like materials because these materials offer access to well-dispersed and homogeneous metallic particles after hydrogen reduction [52-54]. For another, adding another metal to Ni makes higher catalytic activity and enhanced stability of the catalyst possible. The second active metal commonly used can be noble metals such as Ru [55] and Rh [56], or transition metals such as Co [57], Fe [57 58] and Cu [57]. Although

noble metal is even more active than Ni in CO_2 methanation, its large-scale application in real industry is unlikely to happen considering the high cost and limited availability.

To sum up, the biggest challenge to realize CO_2 methanation in industrial scale is to find an appropriate catalyst that balances the catalytic activity, long-term stability, cost and availability.

1.3 Plasma technology

1.3.1 Introduction

Plasma, also known as 'fourth state of matter' together with the other three states of matter 'solid, liquid and gas', widely exists in the universe. It was first introduced by Irving Langmuir in 1927 [59]. Plasma contains not only various types of charged particles (electrons, positive and negative ions) but also a large amount of neutral species (molecules, atoms, radicals and excited species). All species can collide and react with each other, making plasma a highly reactive chemical. This attracts much attention in its applications [60-62]. Nowadays, plasma has been used in material science (coating deposition, surface modification, nanomaterial fabrication), medical treatment (sterilization, wound treatment, cancer treatment), microchip manufacturing and also used as light sources, lasers and displays [63].

Plasma can be widely seen around people. Lightning, auroras or even the sun are in fact plasma. The natural plasma near us includes earth's ionosphere, plasma sphere and the outer magnetosphere [63]. Other than natural plasma, two types of man-made plasma are also well known. One is fusion plasma such as tokomaks and stellarators, another is gas discharges that will be discussed later is this chapter.

Plasma can also be classified into thermal plasma and nonthermal plasma based on whether it is in thermal equilibrium or not. When the temperature of all species in plasma is identical in a localized region, then plasma is in local thermodynamic equilibrium (LTE) and this type of plasma is named thermal plasma. On the contrary, when the temperature of the species in plasma is different (for example, electrons

reach the temperature higher than 10000 °C while at the same time ions and neutrons only achieve gas temperature [64]), then plasma is in non-local thermodynamic equilibrium (non-LTE) and this kind of plasma is named nonthermal plasma. Because most experiments are carried out at temperatures much lower than electron temperature, and DBD-type nonthermal plasma was used in this study, the character of nonthermal plasma is introduced in next session.

1.3.2 Nonthermal plasma

Nonthermal plasma is generated by applying high voltage between two parallel electrodes. As the applied voltage achieves enough high to the so-called breakdown voltage, some gas molecules between electrodes break up to positive ions and electrons. Because the electron is much lighter than the other species in plasma, it can be accelerated by the electric field towards the anode. Thus the electron with high kinetic energy is likely to collide and interact with gas molecules, inducing ionization, dissociation and excitation. The ionization process generates new ions and electrons; the ions also gain energy from electric field and move towards cathode where they result in secondary electron emission. The ionization process and secondary electron emission lead to continuous generation of new electrons, making plasma self-sustaining [63]. The dissociation process generates radicals which are the key components for gas conversion process. The excitation process generates excited molecules which can decay to the ground state accompanied by light emission. Through the above-depicted process, it is possible for gas temperature to maintain close to room temperature while temperature for electrons is relatively high.

The advantages of nonthermal plasma for gas conversion can be summarized as follows. At first, through electron collision, some unexcited gases such as CO_2, can be activated. The electron can easily keep high energy even after collision with other species because it is light so that as it collides with heavier molecules, its energy loss is relatively small. As the electron accumulates the kinetic energy obtained from electric field, CO_2 activation becomes possible. Secondly, the control of conversion

and production becomes more flexible as it is not necessary to heat the entire reactor. The electric field can be managed by simply switching on and off at favorable time. Besides, the power consumption can be easily adjusted and scaled.

There are several types of nonthermal plasma that are usually applied for CO_2 conversion, including dielectric barrier discharge (DBD), gliding arc (GA) discharge, microwave (MW) discharge, radio frequency (RF) discharge, glow discharge (GD), corona discharge, spark discharge and nanosecond pulsed discharge. Among all discharges, DBD was used in this study because of the advantage that it can be operated at atmosphere pressure and easily applied in industry. The detailed introduction to DBD is shown in the next session.

1.3.3 Dielectric barrier discharge (DBD)

DBD is one typical process of nonthermal plasma. It was first introduced by Siemens in his experiment in 1857. The details of DBD history can be found in the review paper by Kogelschatz et al [65]. In the DBD reactor, the dielectric barrier is placed between two planar or concentric electrodes, as indicated in Figure 1.4 [63]. It can prevent sparks and arc generation [66]. DBD is normally operated at pressure of 0.1-10 atm while a frequency of a few Hz to MHz is applied. The discharge gap which gas passes through can be in different size, ranging from 0.1 mm to several cm (0.1 mm: plasma display; 1 mm: ozone generator; several cm: CO_2 lasers) [60 67].

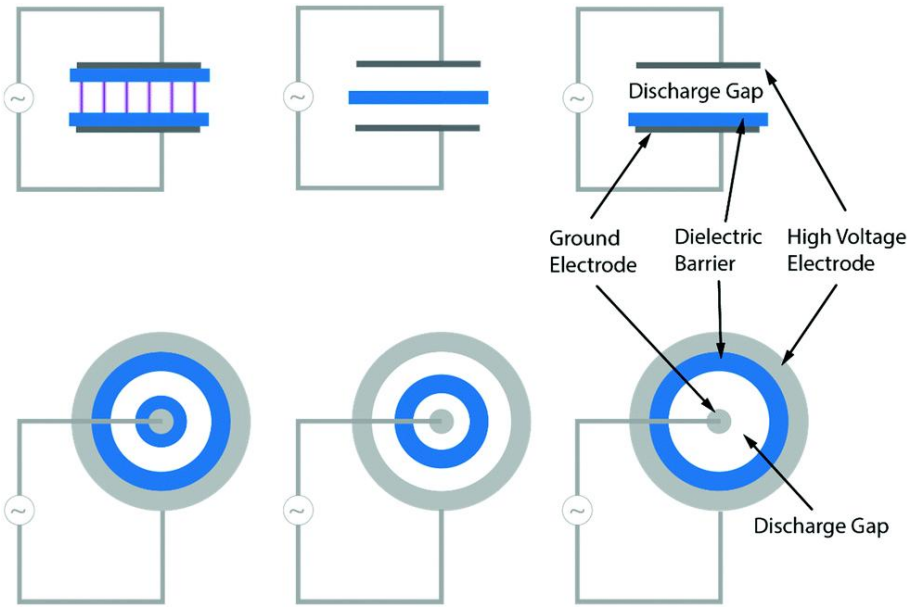

Figure 1.4 Dielectric barrier discharge configurations: basic planar (top) and cylindrical (bottom) [63].

As the applied voltage achieves the breakdown voltage, at most time a non-uniform plasma is generated along with a large quantity of micro-discharges. This process is named 'filamentary mode' which is related to the gas flow inside the discharge region. For CO_2 gas, it can lead to this process. The micro-discharge volume can account for 1-10 % of the total gas volume [68] [69]. During discharge the energetic electrons increase their kinetic energies because they are concentrated inside the filament. This can lead to the dissipation of energy in the dielectric which causes an increase in gas temperature. This also results in the high energy cost and low energy efficiency of DBD-type plasma, which can be seen in Figure 1.5 [30].

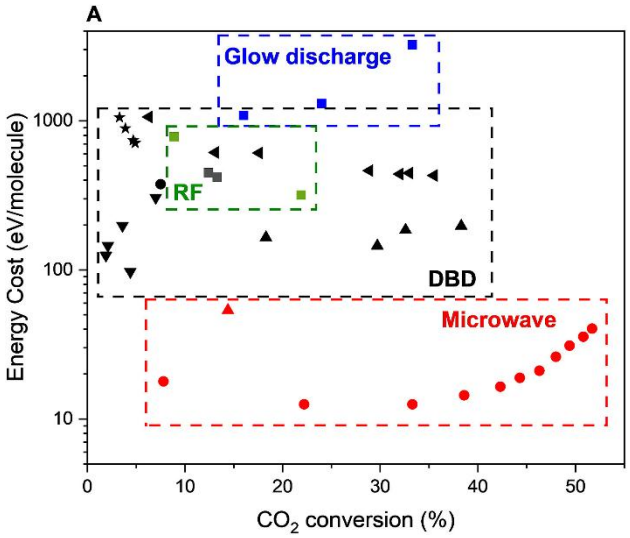

Figure 1.5 Energy cost with respect to CO_2 conversion for different plasma sources and reaction conditions [30]: ■[70], ●[71], ▲[72], ▼[73], ◀[74], ★[75], ■[76], ■[77], ●[78], ▲[79].

1.3.4 Plasma catalysis

Plasma catalysis aims to enhance catalytic reaction by applying plasma to the thermal catalysis system. Theoretically, the combination of plasma and catalysis makes the reaction easier and enhanced. Inert molecules can be activated by plasma under mild conditions. Subsequently activated species selectively recombine on the specific catalyst surface and form the expected products. This is particularly significant for further promoting and optimizing the direct oxidation liquefaction pathway of CO_2 conversion in plasma chemistry. The explanation of interaction between plasma and catalysts can be found in some review papers [80-83].

The possible interaction between plasma and catalyst is depicted in Figure 1.6 [63]. As for the effect of catalyst on plasma, it contains: (1) electric field enhancement due to its surface roughness and geometric structure; (2) micro-discharge formation in pores due to the great electric field in pores; (3) change in discharge type due to the existence of insulating surface; (4) pollutant concentration in plasma due to the increasing residence time. These characters are normally regarded as physical effects. As for the effect of plasma on catalyst, it includes: (1) change of physicochemical properties such as higher adsorption probability on catalyst surface due to the generation of more excited species through plasma; (2) hot spot formation due to the

existence of micro-discharge; (3) activation by photon irradiation due to the excitation process in collision between energetic electrons and gas molecules where light can be emitted; (4) lowering activation barrier; (5) changing surface reaction pathways due to the existence of more active species. These characters are regarded, on the other hand, as effects embracing both physical and chemical natures.

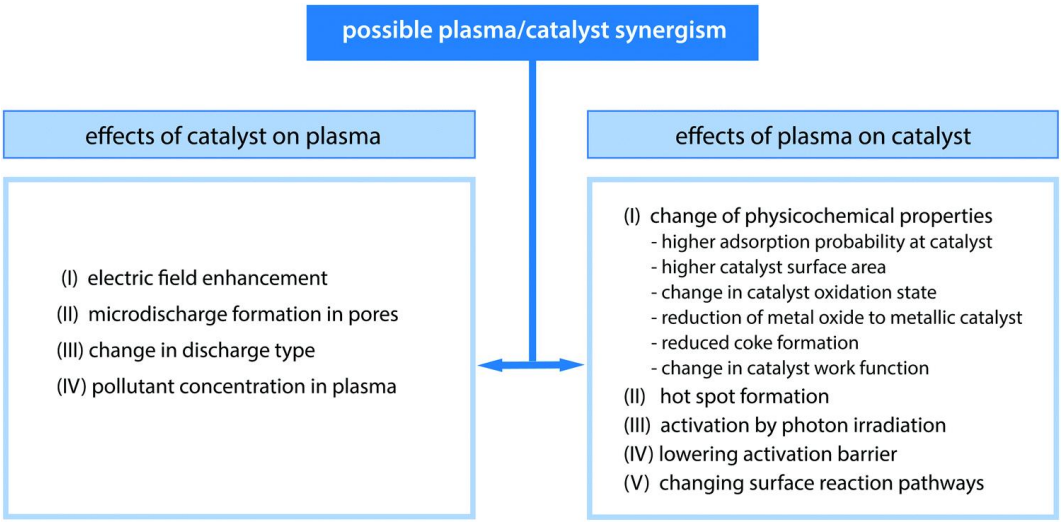

Figure 1.6 The possible interaction between plasma and catalyst [63].

The advantages and disadvantages of plasma catalysis compared with other technologies for gas conversion are shown in Figure 1.7 [63]. The disadvantages of applying plasma technology include: (1) the requirement for product separation after reaction; (2) the energy efficiency determined by the type of reactor; (3) the management of product yield and selectivity under good combination with catalysis. On the other hand, the advantages that plasma technology have contain: (1) unnecessary use of rare earth metals; (2) renewable energy generation by consuming renewable electricity and resources; (3) flexible turnkey process; (4) high CO_2 conversion and product yield; (5) possible generation of oxygenated products; (6) low investment and operating expense; (7) high overall flexibility.

	Use of rare earth metals	Renewable energy	Turnkey process	Conversion and yield	Separation step needed	Oxygenated products (e.g. alcohols, acids)	Investment cost	Operating cost	Overall flexibility
Traditional catalysis	Yes	-	No	High	Yes	Yes	Low	High	Low
Catalysis by MW-heating		Indirect						Low	Low
Electro-chemical	Yes	Indirect	No[b]	High	Yes[c]	Yes	Low	Low	Medium
Solar thermo-chemical	Yes	Direct	NA	High	No	No	High	Low	Low
Photo-chemical	Yes	Direct[a]	Yes	Low	Yes	Yes	Low	Low	Low
Biochemical	No	Direct[a]	No	Medium	Yes[d]	Yes	High /low	High	Low
Plasma-chemical	No	Indirect	Yes	High	Yes[e]	Yes	Low	Low	High

Figure 1.7 The advantage and disadvantage comparison between traditional thermal catalysis and different technologies [63]. Different colors indicate different degrees of influence on a certain feature: negative (red), neutral (orange) and positive (green).

1.4 The scope of the thesis

In plasma-enhanced CO_2 methanation reaction, as nonthermal plasma can provide both heat and radical effect, auto-methanation under nonthermal plasma treatment becomes possible. This thesis aims to demonstrate the feasibility of the above process on different types of catalysts. To this end, plasma-enhanced catalytic performance in the packed-bed dielectric barrier discharge reactor was confirmed at first (Chapter 2). *In situ* diffuse reflectance infrared Fourier-transform spectroscopy experiment was conducted to understand reaction mechanism (Chapter 2). Auto-methanation was designed when discharge power was sufficient for reactor to reach the initial reaction temperature (Chapter 3). DBD plays important roles as 'ignition' and 'promotion' once highly reactive species can well interact with catalyst surface.

Chapter 1 provides the introduction to CO_2 methanation and nonthermal plasma.

The significance of applying nonthermal plasma to CO_2 methanation has been discussed.

Chapter 2 confirms nonthermal plasma-promoted catalytic activity on Ru based multi-metallic catalyst in CO_2 methanation. La-Ni/Al_2O_3 was used as the base catalyst for its good ability to adsorb carbonate species which prove to be the most significant step in CO_2 methanation. Ru was added as the promoter which enhances hydrogen spillover. Because it is known that La provides active sites for CO_2 adsorption. Then Ni-modified Ru/Al_2O_3 was studied to know the effect of Ru and Ni as comparison. The result proves that little plasma promotion effect is found on Ni(Ru)/Al_2O_3 while DBD-enhanced CO_2 conversion is more clearly seen on Ru(La-Ni)/Al_2O_3. Besides, increasing the frequency at constant power further improves the catalytic activity only when La is added to the catalyst, indicating La plays an important role in DBD-enhanced methanation reaction. To understand the reaction pathway on this multi-metallic catalyst, *in situ* diffuse reflectance infrared Fourier-transform spectroscopy was employed. It illustrates the formation of carbonate species and its conversion to CH_4 due to hydrogen spillover on Ru is the key.

Based on the result shown in Chapter 2, DBD-enhanced methanation reaction can be seen on Ru(La-Ni)/Al_2O_3. As DBD provides both heat and radical effect, methanation can happen automatically without any external heating except DBD heating when the catalyst temperature achieves the reaction temperature, namely auto-methanation. Chapter 3 realized auto-methanation process on 4 types of catalysts. To make it come true in real production, scaling up the reactor is always one significant aim in this study. Then 2 indicators including “to see if reaction can be self-sustained after DBD is turned off” and “to see time-dependent change in catalyst temperature distribution” help select the suitable catalyst and analyze the factors that influence successful realization of auto-methanation in large scale reactors. It is found that self-sustained reaction only occurs on both monometallic Ruthenium catalysts due to their good catalytic activities around 200 ° C. This implies the type of catalyst and prevention from heat loss are 2 determining factors when scaling up the reactor. The

catalyst that has good catalytic activity at such low temperature as 200 ℃ is preferred.

Chapter 4 provides conclusion and outlook for the future work.

1.5 References

1 Gerland P, Raftery AE, Ševčíková H, et al. World Population Stabilization Unlikely This Century. *Science*. 2014, **346**: 234-237.

2 Antonakakis N, Chatziantoniou I, Filis G. Energy Consumption, CO_2 Emissions, and Economic Growth: An Ethical Dilemma. *Renewable and Sustainable Energy Reviews*. 2017, **68**: 808-824.

3 Xiaoding X, Moulijn JA. Mitigation of CO_2 by Chemical Conversion: Plausible Chemical Reactions and Promising Products. *Energy & Fuels*. 1996, **10**: 305-325.

4 Mikkelsen M, Jørgensen M, Krebs FC. The Teraton Challenge. A Review of Fixation and Transformation of Carbon Dioxide. *Energy Environ Sci*. 2010, **3**: 43-81.

5 Nema P, Nema S, Roy P. An Overview of Global Climate Changing in Current Scenario and Mitigation Action. *Renewable and Sustainable Energy Reviews*. 2012, **16**: 2329-2336.

6 Yang H, Xu Z, Fan M, et al. Progress in Carbon Dioxide Separation and Capture: A Review. *Journal of Environmental Sciences*. 2008, **20**: 14-27.

7 Cuéllar-Franca RM, Azapagic A. Carbon Capture, Storage and Utilisation Technologies: A Critical Analysis and Comparison of Their Life Cycle Environmental Impacts. *Journal of CO_2 Utilization*. 2015, **9**: 82-102.

8 Gabrielli P, Gazzani M, Mazzotti M. The Role of Carbon Capture and Utilization, Carbon Capture and Storage, and Biomass to Enable a Net-Zero-CO_2 Emissions Chemical Industry. *Industrial & Engineering Chemistry Research*. 2020, **59**: 7033-7045.

9 Bui M, Adjiman CS, Bardow A, et al. Carbon Capture and Storage (CCS): The Way Forward. *Energy & Environmental Science*. 2018, **11**: 1062-1176.

10 Styring P, Jansen D, De Coninick H, et al. *Carbon Capture and Utilisation in the Green Economy*: Centre for Low Carbon Futures New York, NY, USA 2011.

11 Yu KMK, Curcic I, Gabriel J, et al. Recent Advances in CO_2 Capture and Utilization. *ChemSusChem: Chemistry & Sustainability Energy & Materials*. 2008, **1**: 893-899.

12 Götz M, Lefebvre J, Mörs F, et al. Renewable Power-to-Gas: A Technological and Economic Review. *Renewable energy*. 2016, **85**: 1371-1390.

13 Meylan FD, Moreau V, Erkman S. Material Constraints Related to Storage of Future European Renewable Electricity Surpluses with CO_2 Methanation. *Energy Policy*. 2016, **94**: 366-376.

14 Rönsch S, Schneider J, Matthischke S, et al. Review on Methanation–from Fundamentals to Current Projects. *Fuel*. 2016, **166**: 276-296.

15 Thauer RK, Kaster A-K, Seedorf H, et al. Methanogenic Archaea: Ecologically Relevant Differences in Energy Conservation. *Nature Reviews Microbiology*. 2008, **6**: 579-591.

16 Seifert AH, Rittmann S, Herwig C. Analysis of Process Related Factors to Increase Volumetric Productivity and Quality of Biomethane with Methanothermobacter Marburgensis. *Applied Energy*. 2014, **132**: 155-162.

17 Ocampo F, Louis B, Roger A-C. Methanation of Carbon Dioxide over Nickel-Based $Ce_{0.72}Zr_{0.28}O_2$ Mixed Oxide Catalysts Prepared by Sol–Gel Method. *Applied Catalysis A: General*. 2009, **369**: 90-96.

18 Beuls A, Swalus C, Jacquemin M, et al. Methanation of CO_2: Further Insight into the Mechanism over Rh/γ-Al_2O_3 Catalyst. *Applied Catalysis B: Environmental*. 2012, **113**: 2-10.

19 Kopyscinski J, Schildhauer TJ, Biollaz SMA. Production of Synthetic Natural Gas (SNG) from Coal and Dry Biomass–a Technology Review from 1950 to 2009. *Fuel*. 2010, **89**: 1763-1783.

20 Sterner M. *Bioenergy and Renewable Power Methane in Integrated 100% Renewable Energy Systems. Limiting Global Warming by Transforming Energy Systems: Limiting Global Warming by Transforming Energy Systems*: kassel university press GmbH 2009.

21 Brodie BC. Ii. Note on the Synthesis of Marsh-Gas and Formic Acid, and on the Electric Decomposition of Carbonic Oxide. *Proceedings of the Royal Society of London*. 1873, **21**: 245-247.

22 Sabatier P, Senderens JB. Direct Hydrogenation of Oxides of Carbon in Presence of Various Finely Divided Metals. *CR Acad Sci*. 1902, **134**: 689-691.

23 Sikarwar VS, Zhao M, Fennell PS, et al. Progress in Biofuel Production from Gasification. *Progress in Energy and Combustion Science*. 2017, **61**: 189-248.

24 Sreedhar I, Varun Y, Singh SA, et al. Developmental Trends in CO_2 Methanation Using Various Catalysts. *Catalysis Science & Technology*. 2019, **9**: 4478-4504.

25 Aho A, Antonietti M, Arndt S, et al. *Others, Chemical Energy Storage*. Walter de Gruyter 2013.

26 Schaaf T, Grünig J, Schuster M, et al. Speicherung Von Elektrischer Energie Im Erdgasnetz–Methanisierung Von CO_2-Haltigen Gasen. *Chemie Ingenieur Technik*. 2014, **4**: 476-485.

27 Schaaf T, Grünig J, Schuster MR, et al. Methanation of CO_2-Storage of Renewable Energy in a Gas Distribution System. *Energy, Sustainability and Society*. 2014, **4**: 1-14.

28 Younas M, Loong Kong L, Bashir MJK, et al. Recent Advancements, Fundamental Challenges, and Opportunities in Catalytic Methanation of CO_2. *Energy & Fuels*. 2016, **30**: 8815-8831.
29 Muscatello A, Santiago-Maldonado E, editors. Mars in Situ Resource Utilization Technology Evaluation. 2012.
30 Dębek R, Azzolina-Jury F, Travert A, et al. A Review on Plasma-Catalytic Methanation of Carbon Dioxide–Looking for an Efficient Catalyst. *Renewable and Sustainable Energy Reviews*. 2019, **116**: 109427.
31 Gao J, Wang Y, Ping Y, et al. A Thermodynamic Analysis of Methanation Reactions of Carbon Oxides for the Production of Synthetic Natural Gas. *RSC advances*. 2012, **2**: 2358-2368.
32 Lefebvre JEBI. Kit–Ebi Ceb Ebi Ceb-Mitarbeiter. *Fuel Processing Technology*. 2015, **132**: 83-90.
33 Miguel CV, Soria MA, Mendes A, et al. Direct CO_2 Hydrogenation to Methane or Methanol from Post-Combustion Exhaust Streams–a Thermodynamic Study. *Journal of Natural Gas Science and Engineering*. 2015, **22**: 1-8.
34 Su X, Xu J, Liang B, et al. Catalytic Carbon Dioxide Hydrogenation to Methane: A Review of Recent Studies. *Journal of energy chemistry*. 2016, **25**: 553-565.
35 Heine C, Lechner BAJ, Bluhm H, et al. Recycling of CO_2: Probing the Chemical State of the Ni (111) Surface During the Methanation Reaction with Ambient-Pressure X-Ray Photoelectron Spectroscopy. *Journal of the American Chemical Society*. 2016, **138**: 13246-13252.
36 Silaghi M-C, Comas-Vives A, Copéret C. CO_2 Activation on Ni/γ–Al_2O_3 Catalysts by First-Principles Calculations: From Ideal Surfaces to Supported Nanoparticles. *ACS Catalysis*. 2016, **6**: 4501-4505.
37 Vogt C, Groeneveld E, Kamsma G, et al. Unravelling Structure Sensitivity in CO_2 Hydrogenation over Nickel. *Nature Catalysis*. 2018, **1**: 127-134.
38 Vogt C, Monai M, Kramer GJ, et al. The Renaissance of the Sabatier Reaction and Its Applications on Earth and in Space. *Nature catalysis*. 2019, **2**: 188-197.
39 Miao B, Ma SSK, Wang X, et al. Catalysis Mechanisms of CO_2 and CO Methanation. *Catalysis Science & Technology*. 2016, **6**: 4048-4058.
40 Jalama K. Carbon Dioxide Hydrogenation over Nickel-, Ruthenium-, and Copper-Based Catalysts: Review of Kinetics and Mechanism. *Catalysis Reviews*. 2017, **59**: 95-164.
41 Saeidi S, Najari S, Hessel V, et al. Recent Advances in CO_2 Hydrogenation to Value-Added Products — Current Challenges and Future Directions. *Progress in Energy and Combustion Science*. 2021, **85**.

42 Mebrahtu C, Krebs F, Abate S, et al. CO_2 Methanation: Principles and Challenges. *Horizons in Sustainable Industrial Chemistry and Catalysis*. Studies in Surface Science and Catalysis. (2019). p. 85-103.
43 Lim JY, McGregor J, Sederman AJ, et al. Kinetic Studies of CO_2 Methanation over a Ni/γ-Al_2O_3 Catalyst Using a Batch Reactor. *Chemical Engineering Science*. 2016, **141**: 28-45.
44 Fujita S, Terunuma H, Nakamura M, et al. Mechanisms of Methanation of Carbon Monoxide and Carbon Dioxide over Nickel. *Industrial & engineering chemistry research*. 1991, **30**: 1146-1151.
45 Fujita S-i, Nakamura M, Doi T, et al. Mechanisms of Methanation of Carbon Dioxide and Carbon Monoxide over Nickel/Alumina Catalysts. *Applied Catalysis A: General*. 1993, **104**: 87-100.
46 Aldana PAU, Ocampo F, Kobl K, et al. Catalytic CO_2 Valorization into CH_4 on Ni-Based Ceria-Zirconia. Reaction Mechanism by Operando IR Spectroscopy. *Catalysis Today*. 2013, **215**: 201-207.
47 Hubble RA, Lim JY, Dennis JS. Kinetic Studies of CO_2 Methanation over a Ni/γ-Al_2O_3 Catalyst. *Faraday discussions*. 2016, **192**: 529-544.
48 Fogler HS. *Essentials of Chemical Reaction Engineering: Essenti Chemica Reactio Engi*: Pearson Education 2010.
49 Spinicci R, Tofanari A. Comparative Study of the Activity of Titania-and Silica-Based Catalysts for Carbon Dioxide Methanation. *Applied catalysis*. 1988, **41**: 241-252.
50 Kopyscinski J. Production of Synthetic Natural Gas in a Fluidized Bed Reactor: Understanding the Hydrodynamic, Mass Transfer, and Kinetic Effects. 2010.
51 Takezawa N, Terunuma H, Shimokawabe M, et al. Methanation of Carbon Dioxide: Preparation of Ni/MgO Catalysts and Their Performance. *Applied catalysis*. 1986, **23**: 291-298.
52 Feng J-T, Lin Y-J, Evans DG, et al. Enhanced Metal Dispersion and Hydrodechlorination Properties of a Ni/Al_2O_3 Catalyst Derived from Layered Double Hydroxides. *Journal of Catalysis*. 2009, **266**: 351-358.
53 Zhao M-Q, Zhang Q, Zhang W, et al. Embedded High Density Metal Nanoparticles with Extraordinary Thermal Stability Derived from Guest-Host Mediated Layered Double Hydroxides. *Journal of the American Chemical Society*. 2010, **132**: 14739-14741.
54 Ziegler C, Werner S, Bugnet M, et al. Artificial Solids by Design: Assembly and Electron Microscopy Study of Nanosheet-Derived Heterostructures. *Chemistry of Materials*. 2013, **25**: 4892-4900.

55 Ocampo F, Louis B, Kiwi-Minsker L, et al. Effect of Ce/Zr Composition and Noble Metal Promotion on Nickel Based $Ce_xZr_{1-x}O_2$ Catalysts for Carbon Dioxide Methanation. *Applied Catalysis A: General*. 2011, **392**: 36-44.

56 Swalus C, Jacquemin M, Poleunis C, et al. CO_2 Methanation on Rh/γ-Al_2O_3 Catalyst at Low Temperature:"*In Situ*" Supply of Hydrogen by Ni/Activated Carbon Catalyst. *Applied Catalysis B: Environmental*. 2012, **125**: 41-50.

57 Ren J, Qin X, Yang J-Z, et al. Methanation of Carbon Dioxide over Ni–M/ZrO_2 (M= Fe, Co, Cu) Catalysts: Effect of Addition of a Second Metal. *Fuel Processing Technology*. 2015, **137**: 204-211.

58 Pandey D, Deo G. Promotional Effects in Alumina and Silica Supported Bimetallic Ni–Fe Catalysts During CO_2 Hydrogenation. *Journal of Molecular Catalysis A: Chemical*. 2014, **382**: 23-30.

59 Mott-Smith HM. History of "Plasmas". *Nature*. 1971, **233**: 219-219.

60 Bogaerts A, Neyts E, Gijbels R, et al. Gas Discharge Plasmas and Their Applications. *Spectrochimica Acta Part B: Atomic Spectroscopy*. 2002, **57**: 609-658.

61 Fridman A. *Plasma Chemistry*: Cambridge university press 2008.

62 Carreon ML. Plasma Catalysis: A Brief Tutorial. *Plasma Research Express*. 2019, **1**: 043001.

63 Snoeckx R, Bogaerts A. Plasma Technology – a Novel Solution for CO_2 Conversion? *Chemical Society Reviews*. 2017, **46**: 5805-5863.

64 Neyts EC. K.(Ken) Ostrikov, Mk Sunkara, and A. Bogaerts. *Chem Rev*. 2015, **115**: 13408.

65 Kogelschatz U. Dielectric-Barrier Discharges: Their History, Discharge Physics, and Industrial Applications. *Plasma chemistry and plasma processing*. 2003, **23**: 1-46.

66 Tendero C, Tixier C, Tristant P, et al. Atmospheric Pressure Plasmas: A Review. *Spectrochimica Acta Part B: Atomic Spectroscopy*. 2006, **61**: 2-30.

67 Fridman A, Chirokov A, Gutsol A. Non-Thermal Atmospheric Pressure Discharges. *Journal of Physics D: Applied Physics*. 2005, **38**: R1.

68 Aerts R, Somers W, Bogaerts A. Carbon Dioxide Splitting in a Dielectric Barrier Discharge Plasma: A Combined Experimental and Computational Study. *ChemSusChem*. 2015, **8**: 702-716.

69 Bogaerts A, Wang W, Berthelot A, et al. Modeling Plasma-Based CO_2 Conversion: Crucial Role of the Dissociation Cross Section. *Plasma Sources Science and Technology*. 2016, **25**: 055016.

70 Eliasson B, Kogelschatz U, Xue B, et al. Hydrogenation of Carbon Dioxide to Methanol with a Discharge-Activated Catalyst. *Industrial & engineering chemistry research*. 1998, **37**: 3350-3357.

71 Zeng Y, Tu X. Plasma-Catalytic CO_2 Hydrogenation at Low Temperatures. *IEEE Transactions on Plasma Science*. 2015, **44**: 405-411.
72 Zeng Y, Tu X. Plasma-Catalytic Hydrogenation of CO_2 for the Cogeneration of CO and CH_4 in a Dielectric Barrier Discharge Reactor: Effect of Argon Addition. *Journal of Physics D: Applied Physics*. 2017, **50**: 184004.
73 De Bie C, van Dijk J, Bogaerts A. CO_2 Hydrogenation in a Dielectric Barrier Discharge Plasma Revealed. *The Journal of Physical Chemistry C*. 2016, **120**: 25210-25224.
74 Mora EY, Sarmiento A, Vera E, editors. Alumina and Quartz as Dielectrics in a Dielectric Barrier Discharges DBD System for CO_2 Hydrogenation. 2016: IOP Publishing.
75 Bacariza MC, Biset-Peiró M, Graça I, et al. DBD Plasma-Assisted CO_2 Methanation Using Zeolite-Based Catalysts: Structure Composition-Reactivity Approach and Effect of Ce as Promoter. *Journal of CO_2 Utilization*. 2018, **26**: 202-211.
76 Kano M, Satoh G, Iizuka S. Reforming of Carbon Dioxide to Methane and Methanol by Electric Impulse Low-Pressure Discharge with Hydrogen. *Plasma Chemistry and Plasma Processing*. 2012, **32**: 177-185.
77 Arita K, Iizuka S. Production of CH_4 in a Low-Pressure CO_2/H_2 Discharge with Magnetic Field. *Journal of Materials Science and Chemical Engineering*. 2015, **3**: 69.
78 de la Fuente JF, Moreno SH, Stankiewicz AI, et al. Reduction of CO_2 with Hydrogen in a Non-Equilibrium Microwave Plasma Reactor. *International Journal of Hydrogen Energy*. 2016, **41**: 21067-21077.
79 Chen G, Britun N, Godfroid T, et al. Efficient CO_2 Conversion in Microwave Plasma Via Plasma Catalysis. *J Phys D: Appl Phys*. 2017, **50**: 084001.
80 Chen HL, Lee HM, Chen SH, et al. Removal of Volatile Organic Compounds by Single-Stage and Two-Stage Plasma Catalysis Systems: A Review of the Performance Enhancement Mechanisms, Current Status, and Suitable Applications. *Environmental science & technology*. 2009, **43**: 2216-2227.
81 Neyts EC, Bogaerts A. Understanding Plasma Catalysis through Modelling and Simulation—a Review. *Journal of Physics D: Applied Physics*. 2014, **47**: 224010.
82 Neyts EC, Ostrikov K, Sunkara MK, et al. Plasma Catalysis: Synergistic Effects at the Nanoscale. *Chemical reviews*. 2015, **115**: 13408-13446.
83 Whitehead JC. Plasma–Catalysis: The Known Knowns, the Known Unknowns and the Unknown Unknowns. *Journal of Physics D: Applied Physics*. 2016, **49**: 243001.

Chapter 2: CO_2 methanation with DBD treatment over multi-metallic Ru based catalyst

This chapter is adapted from the published work:

Zhan, C.; Kim, D.; Xu, S.; Kim, H.; Nozaki, T., Nonthermal plasma catalysis of CO_2 methanation over multi-metallic Ru based catalysts. *International Journal of Plasma Environmental Science and Technology*, 2022, **16**, e03006

2.1 Abstract

This chapter illustrates nonthermal plasma effect on CO_2 methanation over Ru based multi-metallic catalysts. CO_2 conversion behavior in a packed-bed dielectric barrier discharge (PB-DBD) reactor at 100 kPa and 30 kPa with catalyst temperature between 100 °C and 400 °C were investigated and compared with thermal catalysis. The low-temperature CO_2 methanation was improved by Ru-based multi-metallic catalyst and applying DBD to the reaction. Overall methanation performance was improved by La because adsorption of vibrationally excited CO_2 over La sites is enhanced. Besides, increasing the frequency from 12 kHz to 100 kHz at constant power can improve reaction performance because high-frequency operation enhances generation of vibrationally excited CO_2, further accelerating carbonate formation on catalysts. To better understand reaction mechanism in DBD environment, *in situ* diffuse reflectance infrared Fourier-transform spectroscopy (DRIFTS) was employed under the presence of DBD. Formation of carbonate species and its conversion to CH_4 due to hydrogen spillover on Ru is the key reaction pathway in DBD-enhanced methanation reaction.

2.2 Introduction

CO_2 methanation is considered as one promising way to produce synthetic renewable methane at high yield by using renewable hydrogen [1]. However, this reaction is affected by slow conversion speed at low temperatures because the high thermodynamic stability of CO_2 leads to a high activation barrier for its dissociation [2]. To accelerate the low-temperature CO_2 conversion, three approaches of photocatalysis [3, 4], electrocatalysis [4-6] and nonthermal plasma catalysis [4, 7-9] powered by renewable sources, referred to as *Power-to-Chemicals* (PtC), can be adopted. Among these three methods, nonthermal plasma catalysis is an emerging-type new approach which would realize better product yield at low cost [10]. Although CO_2 methanation favors high pressure environment, studying it at reduced pressure avoids various problems. First, the parasite discharge is avoided where gas breakdown occurs at the outside of the reactor (near the sharp edge of grounded electrode). Second, thermal runaway is minimized where the catalyst temperature increases rapidly. Third, gas breakdown occurs rather uniformly which avoids intense and localized gas breakdown. These issues are discussed in detail in section 2.5.

Ni-based catalyst is widely adopted in CO_2 methanation due to its good compromise between catalytic activity, cost, processability, and environmental compatibility [11]. However, some problems remain, such as a high reaction temperature is normally the prerequisite for maximum CO_2 conversion; and the deactivation can occur due to the interaction between Ni-particles and reactive CO as well as the formation of mobile nickel subcarbonyls [12, 13]. This results in undesired influences on the lifetime of the catalysts and increased energy consumption. To solve this problem, some noble metals of Ru, Rh, Pd and Pt, are added to improve the catalytic activity and stability as these metals exhibit good resistant properties to carbon deposition, which can protect the active phase of catalysts from being sintered [14]. Therefore, recent studies mostly focus on catalytic performance of bimetallic and multi-metallic catalysts [11, 15-17]. Although, Ru is the key component of CO_2 methanation, yielding methane at high selectivity, reaction enhancement by DBD with

Ni-Ru catalyst was not significant in our study. Because Ru does not promote CO_2 fixation on the surface as intermediate species such as carbonates. Meantime, the effectiveness of La was proven in our previous study that it enhances carbonate formation under DBD condition. Therefore, in this chapter, the reactivity of "Ni-Ru" and "La-Ni-Ru" catalysts under DBD environment is studied so that the individual contribution of Ru and La is clarified. Moreover, to evaluate DBD-enhanced reaction promotion effect appropriately, the pulsed reforming is introduced at reduced pressure in which gas flow and DBD are applied intermittently so that unexpected temperature raise due to heat generation by DBD as well as methanation is avoided. To understand the plasma-induced reaction enhancement mechanism, in situ diffuse reflectance infrared Fourier-transform spectroscopy (DRIFTS) study is employed.

2.3 Catalyst preparation and characterization

Ru-modified La-Ni/Al_2O_3 catalyst, herein expressed as “Ru(La-Ni)/Al_2O_3”, was employed in this chapter. La-Ni/Al_2O_3 (Rasching ring: 3×3 mm (diameter×height) with 1 mm hole) was used as base catalyst and Ru was added as a reaction promoter. La plays the key role to increase carbonate species on La-Ni-Al complex oxide via vibrationally activated CO_2 [18]. Ru was loaded by an impregnation method using Ru(III) nitrosyl nitrate standard solution (1.5% Ru). The La-Ni/Al_2O_3 Rasching ring was added to a flask containing the Ru precursor solution and held at room temperature for 12 h before drying in a rotary evaporator. The catalysts were calcined in air at 500°C for 10 h and finally reduced in 5% H_2 (Ar balance) at 600°C for 1h. The Ni, La and Ru loading are 11 wt%, 3 wt% and 1 wt%, respectively. Another catalyst of Ni-modified Ru/Al_2O_3, herein expressed as “Ni(Ru)/Al_2O_3”, was employed as a control catalyst. Ru/Al_2O_3 (Regular cylindrical pellet: 3×3 mm (diameter×height)) was used as base catalyst and Ni was loaded by an impregnation method using $Ni(NO_3)_2 \cdot 6H_2O$ as precursor. The conditions of calcination and reduction are the same as Ru(La-Ni)/Al_2O_3. The elemental composition of the prepared catalysts was

analyzed with energy-dispersive X-ray fluorescence (XRF, Rigaku EDXL300). Ni and Ru loading are 10 wt% and 1 wt%, respectively.

High-angle Annular Dark Field Scanning Transmission Electron Microscopy (HAADF-STEM) and energy dispersive X-ray spectroscopy (EDS) were carried out to obtain the element distributions on catalyst. Catalyst pellets were crushed by mechanical milling and reduced prior to the analysis. Figure 2.1 shows the element mapping of Ru(La-Ni)/Al_2O_3, where Ru, La, and Ni are identified in Figure 2.1(b)-(d). Because Ni and La produce a complex La-Ni-Al oxide support, the distribution of these elements is rather uniform. Meantime, Ni produces fine particles simultaneously, which are recognizable in Figure 2.1(a) and (d). The boundary of Ni nanoparticles is not clearly visible because La-Ni-Al oxide is overlapped; therefore, XRD analysis was applied, showing the mean size of Ni particles was ca. 11 nm, while La was mostly in the oxide form (no La fine particles were recognized) [18]. Ru fine particles are identified in Figure 2.1(b): Ni, La, and Ru are found well overlapped. Because the proximity of metallic components determines the cooperative effect in multi-metallic catalysts [19], synergistic interaction between active species on these three metals can occur to enhance the reaction.

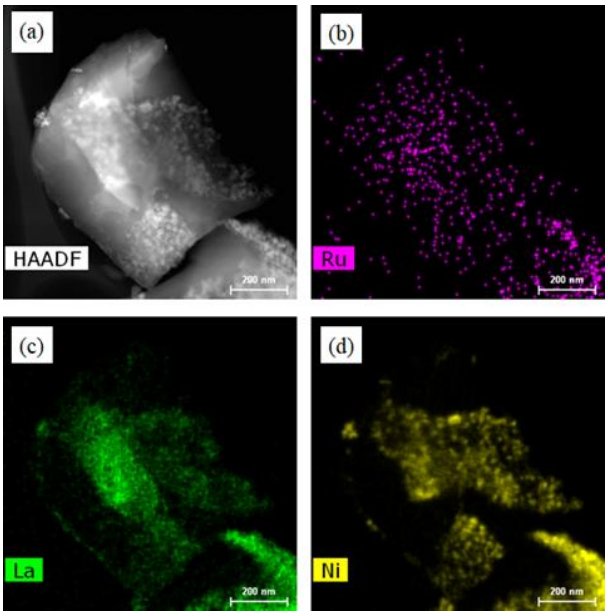

Figure 2.1 (a) HAADF-STEM image of Ru(La-Ni)/Al_2O_3 and (b-d) element mapping

by EDS.

2.4 Experimental system and conditions

Figure 2.2 shows the schematic diagram of experimental setup while experimental parameters are listed in Table 2.1. Definition of Weight Hourly Space Velocity (WHSV; $cm^3/g/h$) and Specific Energy Input (SEI; eV/molecule) are provided as follows:

$$WHSV = \frac{60 \times Q_{\text{total}}^{\text{in}}}{W} \tag{R2.1}$$

$$SEI = \frac{power}{eN_{\text{A}} \times \frac{Q_{\text{total}}^{\text{in}}}{60 \times 10^6} \times \frac{P}{RT}} \tag{R2.2}$$

$Q_{\text{total}}^{\text{in}}$ (cm^3/min) represents total gas flow rate at standard condition (T = 25 °C and P = 101 kPa); W (g) is the catalyst weight; $e = 1.602 \times 10^{-19}$ (C); $N_{\text{A}} = 6.02 \times 10^{23}$; R = 8.314 J/K/mol.

The catalyst pallets are fully packed in the discharge region (40 mm in length) of a packed-bed dielectric barrier discharge (PB-DBD) reactor which is a quartz tube with inner diameter of 20 mm. The high-voltage electrode (3 mm diameter) is laid at the tube center and the ground electrode is placed outside the tube. DBD was generated in the packed-bed region by applying a high voltage power source (12 kHz and 100 kHz). Discharge power, kept at 30 W in this chapter, was determined by voltage-charge Lissajous analysis. Prior to each catalytic experiment, 13.4 g of catalysts were reduced at 500 °C by a constant 10 vol% of H_2/Ar stream for 1.5 h. Then the catalytic experiments were conducted at fixed pressure of 100 kPa or 30 kPa with temperature from 100 °C to 400 °C. Reaction temperature was measured by the infrared camera（TH5104; NEC Sanei Instrument Ltd.) and controlled by an electrical furnace equipped with a temperature controller at a constant heating rate of 2 °C/min.

H_2 and CO_2 in total flow rate of 1200 cm^3/min were mixed at a H_2:CO_2 molar ratio of 5:1. A quadruple mass spectrometer (QMS: PrismaPlus; Pfeiffer Vacuum GmbH) was used for online gas measurement. Conversion and selectivity of each species in CO_2 methanation were calculated by the following equations (R2.3-R2.6), where F^{in} and F^{out} represent molar flow rate (mol/s) of each gas at the inlet and outlet of the reactor, respectively. Reaction product was CH_4 with 100% selectivity which was confirmed by the carbon balance. No other by-products, such as coke, tar, liquid hydrocarbons, or higher hydrocarbons (C_nH_m: n > 2, m > 2) were detected.

$$CO_2 \text{ conversion } (\%) = \frac{F^{in}_{CO_2} - F^{out}_{CO_2}}{F^{in}_{CO_2}} \times 100 \quad \text{(R2.3)}$$

$$H_2 \text{ conversion } (\%) = \frac{F^{in}_{H_2} - F^{out}_{H_2}}{F^{in}_{H_2}} \times 100 \quad \text{(R2.4)}$$

$$CH_4 \text{ selectivity } (\%) = \frac{F^{out}_{CH_4}}{F^{in}_{CO_2} - F^{out}_{CO_2}} \times 100 \quad \text{(R2.5)}$$

$$CO \text{ selectivity } (\%) = \frac{F^{out}_{CO}}{F^{in}_{CO_2} - F^{out}_{CO_2}} \times 100 \quad \text{(R2.6)}$$

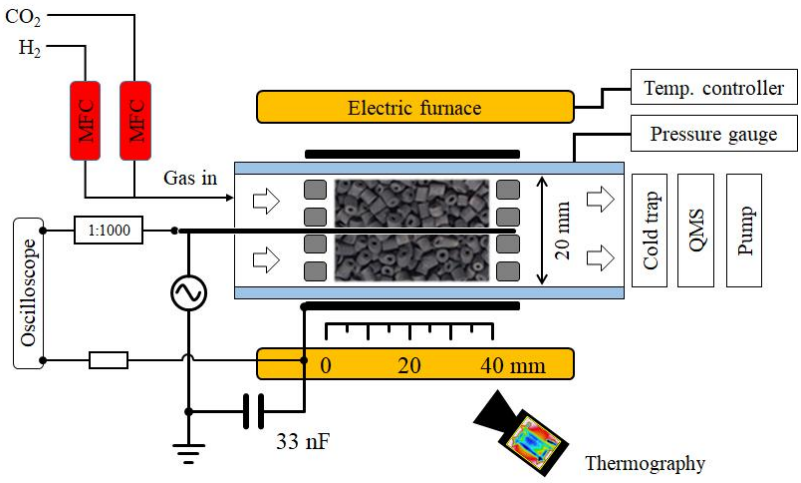

Figure 2.2 Experimental system with horizontal PB-DBD reactor

Table 2.1 Experimental conditions. Catalyst temperature: 100-400 °C; Pressure: 100 kPa and 30 kPa.

	Total flow (cm^3/min)	Catalyst weight (g)	WHSV (cm^3/g/h)	Power (W)	Frequency (kHz)	SEI (eV/molecule)
Plasma catalysis	1200 (H_2/CO_2 = 5)	13.4	5373	30	12, 100	0.38
Thermal catalysis				Not applicable		

2.5 Enhanced CO_2 conversion by nonthermal plasma

Although the catalyst temperature is increased at constant heating rate (2 °C/min), exothermic CO_2 methanation leads to the thermal runaway that causes uncontrolled abrupt temperature increase. Thermal runaway becomes even more intense with DBD because of two reasons. First, DBD promotes CO_2 methanation reaction compared to thermal reaction. Second, heat generated by DBD contributes to temperature increase. To prevent the rapid temperature increase in plasma catalysis, pulsed methanation was used. The catalytic performance in this chapter is evaluated by the value of T_{50}, which corresponds to the temperature at which 50% of CO_2 conversion is attained. A lower T_{50} value is expected when DBD is applied.

2.5.1 Pulsed methanation

Pulsed methanation is the combination of cyclic DBD operation and periodic gas supply [20]. This prevents thermal runaway where catalyst temperature increases abruptly in an uncontrollable manner. During DBD is off, methanation is weakened; thus rapid temperature increase is suppressed. Likewise, during H_2 flow is off, methanation reaction ceases so that rapid temperature increase is suppressed. As a result, CO_2 and H_2 conversions as well as CH_4 yield were obtained at each temperature points. Figure 2.3

indicates the example of time-dependent change in gas composition for pulsed plasma catalysis over Ru(La-Ni)/Al_2O_3 at a certain period. As schematically shown in Figure 2.3(a), H_2 was supplied for 4 min at H_2/CO_2 = 5, then H_2 flow was turned off for 2 min. Meantime, DBD was ON and OFF at a constant interval of 1 min (Figure 2.3(b)). Catalyst temperature (*T*) either increase or decrease temporarily depending on the combination of H_2 flow and DBD operation. Detailed description of operation conditions and catalyst temperature behavior is provided in Table 2.2. Reforming data at the third minute of each H_2-ON process (at *d* point) was selected for gas analysis as the signal in QMS gets stable. As clearly seen in Figure 2.3(c), catalyst temperature fluctuation during DBD-ON period is greater than furnace heating rate (2 °C/min); therefore, the pulsed methanation technique is necessary to avoid thermal runaway and extract the DBD promotion effect properly. During H_2-OFF period, only CO_2 was supplied at 500 cm^3/min to cease the methanation temporarily and cool down the catalyst temperature.

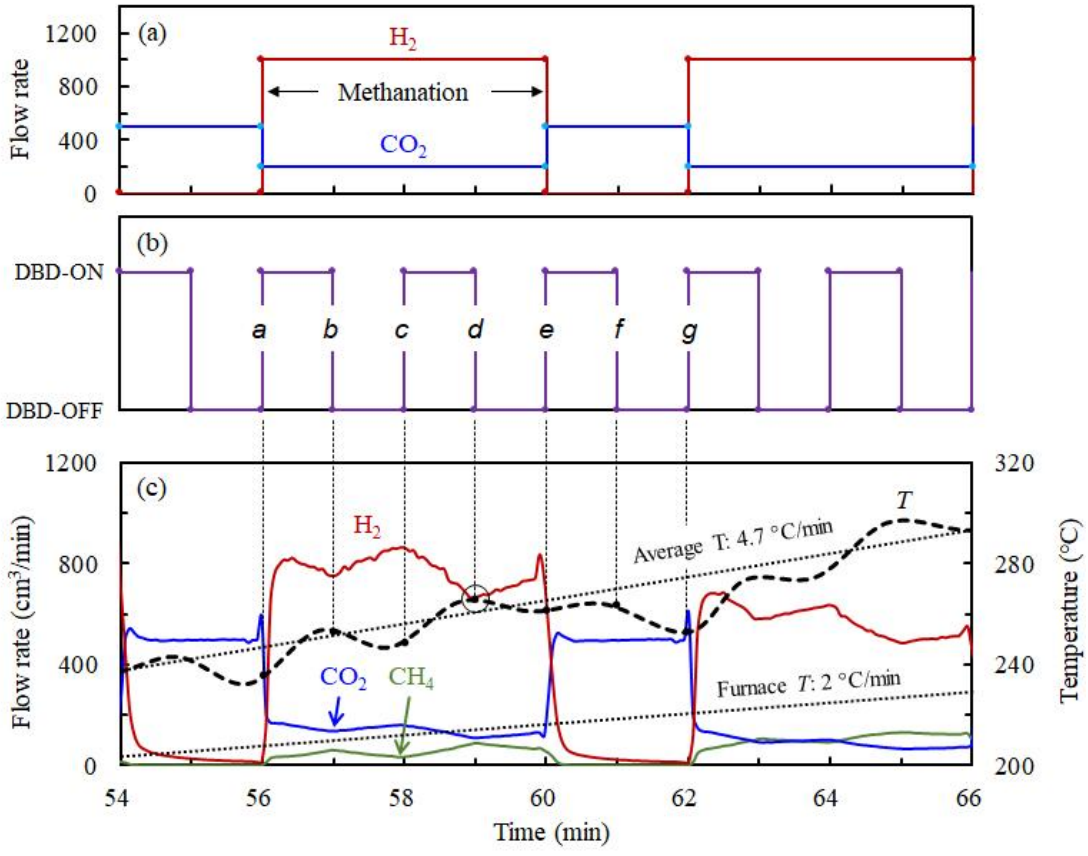

Figure 2.3 Pulsed methanation at a certain period. (a) pulsed gas-supply; (b) pulsed DBD; (c) Time-dependent change in gas composition and catalyst temperature.

Table 2.2 Detailed description of catalyst temperature variation during pulsed methanation.

	Time	DBD	H_2 (cm^3/min)	CO_2 (cm^3/min)	Temperature profile
Methanation	*a-b*	ON	1,000	200	d*T*/dt > 0 Catalyst temperature (*T*) increases rapidly due to DBD heating and DBD-promoted methanation.
	b-c	OFF			d*T*/dt < 0 Reaction promotion by DBD is absent. DBD heating is also absent. Although heat generation by methanation (thermal catalysis) is possible, it is not sufficient to maintain reaction temperature which decreases without DBD.
	c-d	ON			d*T*/dt > 0 Same as "*a-b*" period. Data acquisition by QMS at Point *d*: CO_2 conversion = 44.4 %, reaction heat = 10 W (Figure 2.3(c)).
	d-e	OFF			d*T*/dt < 0 Same as "*b-c*" period.
w/o reaction	*e-f*	ON	0	500	d*T*/dt > 0 *T* increases slightly by DBD heating. The heating effect is moderate compared to the "*a-b*" and "*c-d*" periods because methanation is absent (H_2 = 0 cm^3/min).
	f-g	OFF			d*T*/dt < 0 *T* decreases due to the absence of neither methanation nor DBD. Comparing the "*e-f*" and "*f-g*" periods, the DBD heating effect (30 W) is remarkable (Figure 2.4(c)).

2.5.2 Effect of pressure

First, CO_2 methanation performance at 100 kPa was studied. Figure 2.4(a) shows CO_2 conversion over two types of catalysts and compares the results with thermodynamic equilibrium. With DBD treatment, T_{50} is lowered slightly from 275 °C (blue line) in thermal reaction to 257 °C (red line) over Ru(La-Ni)/Al_2O_3 and is decreased from 292 °C (yellow) to 278 °C (black) over Ni(Ru)/Al_2O_3. The catalytic performance of Ru(La-Ni)/Al_2O_3 is better and the low-temperature CO_2 methanation is improved by DBD. Our previous study showed that La enhances CO_2 adsorption as carbonates and the vibrationally excited CO_2 would promote such reaction [18, 20, 21]. When catalyst temperature reaches 350 °C, due to equilibrium limitation, there is no clear difference between thermal and plasma catalysis over respective catalysts. Meantime, conversion on Ru(La-Ni)/Al_2O_3 reaches much closer to equilibrium than that of Ni(Ru)/Al_2O_3, suggesting that La gives rise to a better catalytic activity. Figure 2.4(b) shows H_2 conversion with temperature: H_2 conversion behavior is quite similar to that of CO_2. Therefore, Only CO_2 conversions are discussed in the following sections.

Figure 2.4(c) shows the heat generation by methanation calculated by R2.7, assuming CH_4 selectivity is 100% based on the experimental results.

$$\text{Reaction heat} = \left(F_{CO_2}^{in} - F_{CO_2}^{out}\right) \times \Delta H_f^{\circ} \times 10^{-3} \text{ (W)} \qquad \text{(R2.7)}$$

Discharge power (30 W) was larger than the exothermic reaction heat over the catalyst temperature. Obviously, the catalyst temperature is higher than the temperature of the electric furnace. Thermal insulation of the packed-bed DBD reactor and heat transfer control need to be optimized so that the plasma-induced reaction promotion is optimized.

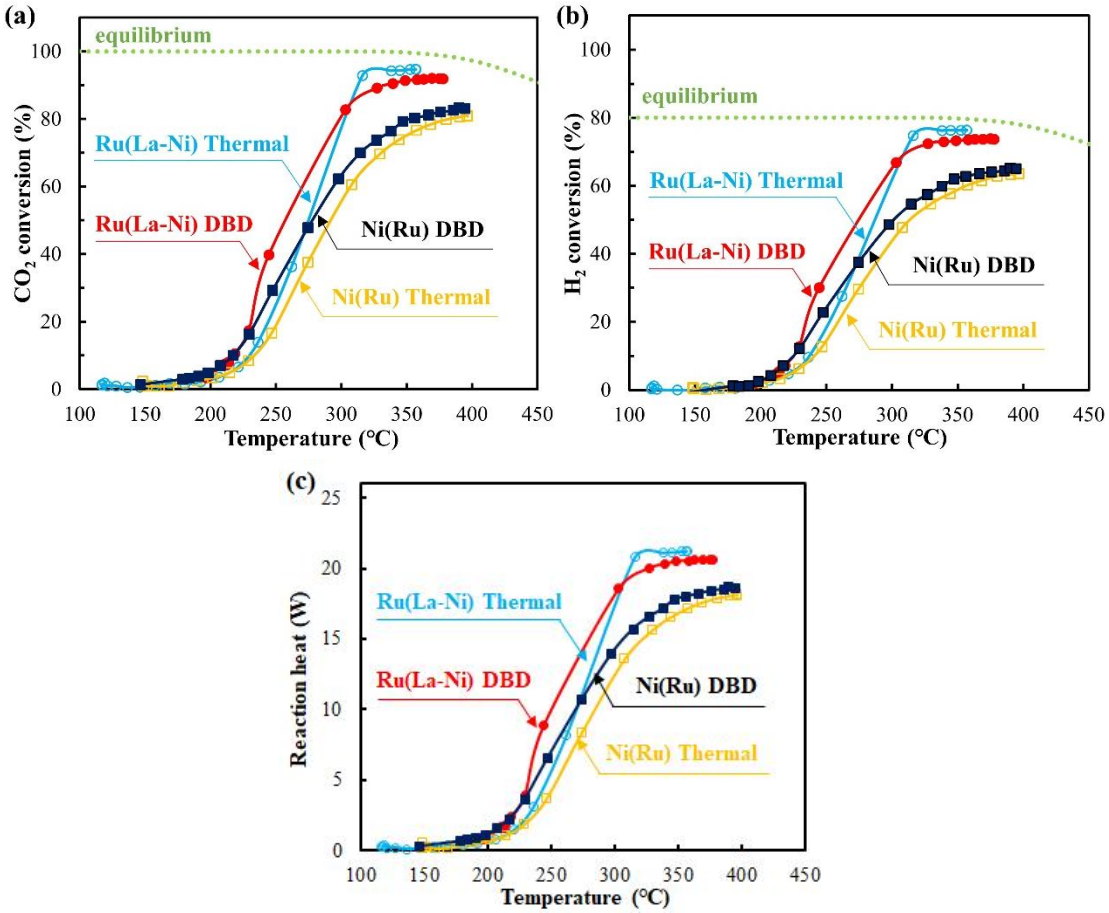

Figure 2.4 Catalytic activity on Ru(La-Ni)/Al_2O_3 and Ni(Ru)/Al_2O_3 at 100kPa with and without DBD: (a) CO_2 conversion and (b) H_2 conversion, (c) heat generated by methanation, respectively.

According to the thermal equilibrium, the higher the reaction pressure is, the higher the CO_2 conversion. However, three issues remain in plasma catalysis. First, discharge at pressure higher than atmospheric pressure generates localized and intense gas breakdown that damages the catalysts. Second, gas breakdown more likely occurs outside of the reactor, known as *parasite discharge*. This will weaken discharge inside reactor. Third, much reaction heat is released under higher pressure which causes serious thermal runaway even with application of pulsed methanation. The third problem is the most critical and can be seen in Figure 2.4, for Ru(La-Ni)/Al_2O_3 at 100 kPa (in red and blue), less experimental data was obtained from 220 °C to 300 °C because catalyst temperature increased rapidly in a shorter period of time due to the intensive methanation reaction at 100 kPa. To avoid these problems, experiments were

carried out at a lower pressure of 30 kPa.

Figure 2.5 compares the catalytic performance of Ru(La-Ni)/Al_2O_3 and Ni(Ru)/Al_2O_3 at 30 kPa. Equilibrium CO_2 conversion at 30 kPa and 100 kPa is also shown in Figure 2.5. Similar to Figure 2.4, the onset temperature is ca. 200 °C and not influenced by the type of catalyst and the application of DBD. CO_2 conversion reaches the maximum limit of 75% in all four cases. Experimental CO_2 conversion at 30 kPa is obviously lower than that of 100 kPa, while equilibrium conversion is not influenced markedly by 30 kPa and 100 kPa. This is caused by the reduction of the net reaction time which is shortened as pressure decreases. When the total gas flow rate decreases so that the net reaction time is equivalent to 100 kPa operation, CO_2 conversion at 30 kPa was close value to that of 100 kPa (data is not shown). One noticeable superiority of Ru(La-Ni)/Al_2O_3 is that CO_2 conversion develops at lower temperature than Ni(Ru)/Al_2O_3, and reaches the maximum limit at around 300 °C. Reaction promotion by DBD is observed clearly when CO_2 conversion is much lower than the equilibrium. To further investigate the DBD-induced synergistic effect, frequency of 100 kHz was studied at fixed pressure of 30 kPa.

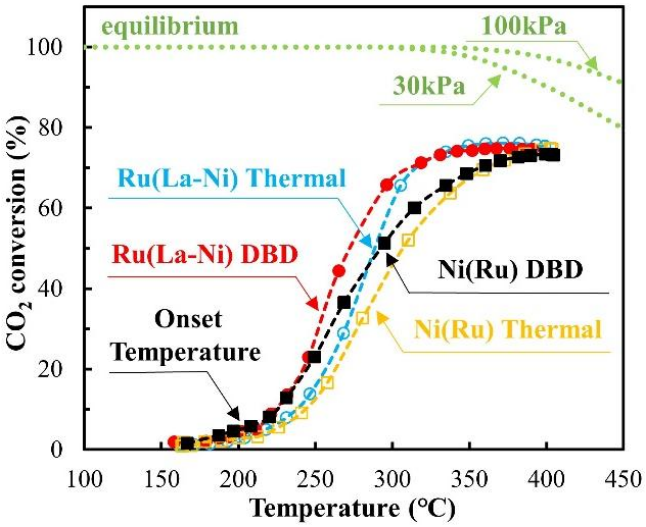

Figure 2.5 Comparison of catalytic performance on Ni(Ru)/Al_2O_3 and Ru(La-Ni)/Al_2O_3 at 30 kPa.

2.5.3 Effect of frequency

In our previous study, 100 kHz operation was more effective than 12 kHz because higher frequency increases the mean discharge current without increasing the discharge power [21]. As a result, generation of vibrationally excited CO_2 increases without gas heating. More importantly, DBD is generated per half cycle of frequency which would be faster than the quenching rate of vibrational species: vibrationally excited species would be accumulated in high frequency operation and interact with catalyst even during discharge-off period. The comparison results are shown in Figure 2.6. For Ni(Ru)/Al_2O_3, the promotion of CO_2 conversion by increasing frequency is negligible. However, for Ru(La-Ni)/Al_2O_3, the synergistic effect is clearly observed. Compared to T_{50} value of 272 °C in the case of 12 kHz, a clear reduction to 250 °C is obtained when 100 kHz is applied. For Ru(La-Ni)/Al_2O_3, more carbonates are generated on La-Ni-Al complex oxide [18, 23, 24]. La provides additional active sites for CO_2 adsorption. However, due to the small content of Ru, CO_2 adsorption on Ru in Ni(Ru)/Al_2O_3 will not be influenced by the frequency. As Ru(La-Ni)/Al_2O_3 showed better catalytic performance than Ni(Ru)/Al_2O_3, the reaction mechanism was explored by *in situ* infrared absorption spectroscopy using Ru(La-Ni)/Al_2O_3.

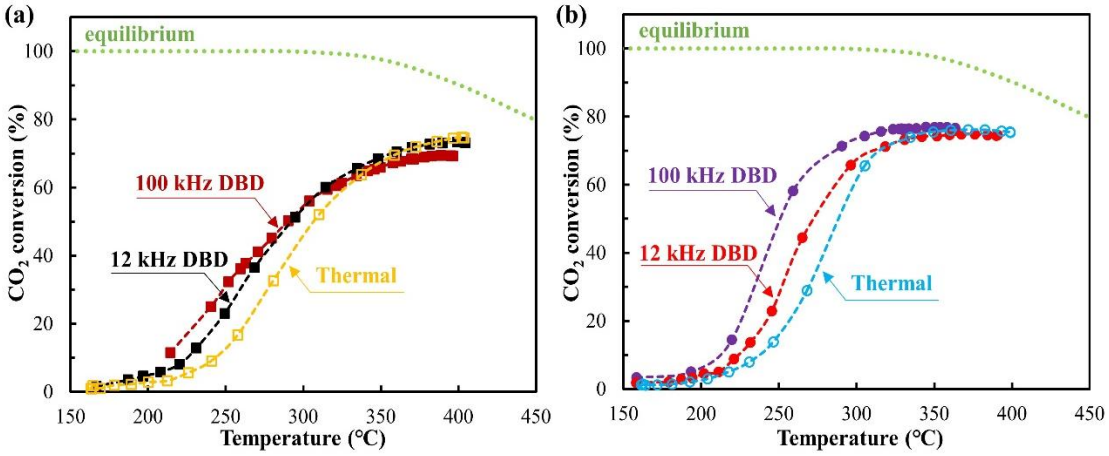

Figure 2.6 Comparison of catalytic performances at different frequency at 30 kPa over (a) Ni(Ru)/Al_2O_3 and (b) Ru(La-Ni)/Al_2O_3.

2.6 *In situ* DRIFTS study

In situ DRIFTS (diffuse reflectance infrared Fourier transform spectroscopy)

analysis was conducted to understand the plasma-induced reaction enhancement mechanism [25]. The detailed experimental setup was reported in our previous work [18]. Briefly, FTIR (Perkin Elmer, Frontier) equipped with a mercury cadmium telluride (MCT) detector was used for the DRIFTS analysis. The catalyst powder was pretreated in the DRIFTS cell at 500 °C for 30 min under H_2/He = 50/50 cm^3/min flow. The catalyst temperature was set to 300 °C under the pure helium flow, then DRIFTS spectra were recorded by various gas-flow conditions with and without DBD irradiation.

Figure 2.7 illustrates the DRIFTS spectra of CO_2 adsorption and methanation reaction over Ru(La-Ni)/Al_2O_3. The structure of carbonate and the other intermediate species coordinated with La is summarized in Table 2.3. Generally, IR absorption by functional groups is characterized by multiple peaks, not a single peak. For example, monodentate carbonate is characterized by different vibrations as 1360 and 1425 cm^{-1}. Although these peaks are not clearly distinguished in Figure 2.7(a1), these two peaks must be assumed during deconvolution of overlapped spectra. If a single peak is assumed, such as 1360 cm^{-1} only, it could be an inconsistent analysis, ignoring other peaks (e.g. 1425 cm^{-1}) which should co-exist.

Figure 2.7(a1) was obtained after 20 min exposure to the pure CO_2 flow (40 cm^3/min). Subsequently, DBD was turned on for 20 min then spectrum was recorded as a plasma catalytic reaction (Figure 2.7(a2)). The bands at 1360 and 1425 cm^{-1} are monodentate carbonate (m-CO_3^{2-}); the band at 1540 cm^{-1} is assigned to bidentate carbonate (b-CO_3^{2-}) [26-28]. When DBD is applied, the peak intensity of m- and b-carbonate are clearly increased: the total area of these carbonates in plasma catalysis increased an approximately 1.75-fold compared to the thermal catalysis. After CO_2-DBD treatment, CO_2/H_2 (= 40/60 cm^3/min) mixture was introduced to the DRIFTS cell and the spectrum was recorded in 20 min without DBD (Figure 2.7(b1)). Subsequently, DBD was applied and the spectrum was obtained in 20 min (Figure 2.7(b2)). When H_2 and CO_2 were introduced simultaneously, bidentate carbonate (1540 cm^{-1}) disappears; instead, polydentate carbonate (p-CO_3^{2-}: 1395 and 1510 cm^{-1})

and formyl (HCO: 1740 cm^{-1}) appear [29-32]. The observation suggest hydrogen reacts primarily with bidentate carbonate to generate polydentate carbonate and formyl. When DBD is applied, this reaction was promoted and the peak intensity of all peaks were increased (Figure 2.7(b)). In comparison, the area of formyl increases by 1.5-fold with DBD treatment.

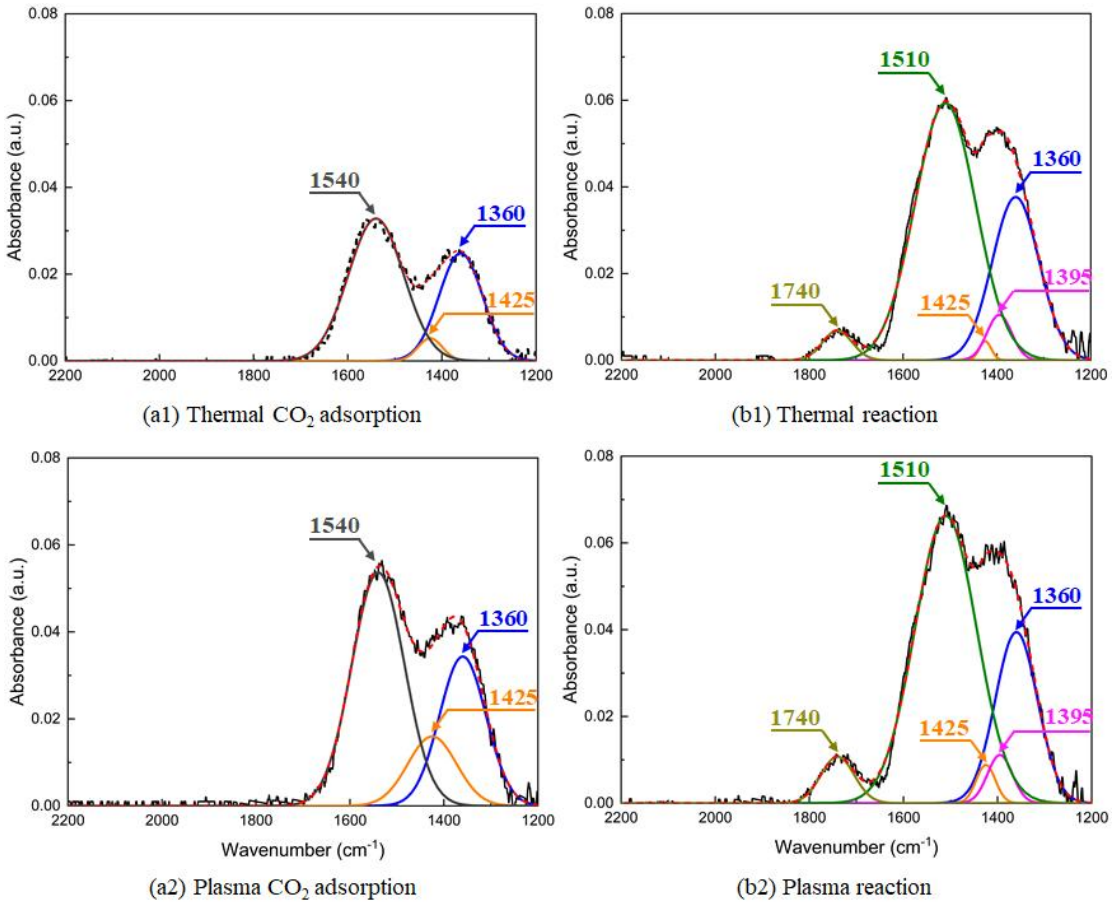

Figure 2.7 *In situ* DRIFTS spectra at 300 °C of CO_2 adsorption: (a1) thermal and (a2) plasma. CO_2 methanation: (b1) thermal and (b2) plasma. Monodentate carbonate (1360 and 1425 cm^{-1}); Bidentate carbonate (1540 cm^{-1}); Polydentate carbonate (1395 and 1510 cm^{-1}); Formyl (1740 cm^{-1}).

Table 2.3 The structure of intermediate species found in *In situ* DRIFTS study (*M represents the coordination metal, lanthanum in this chapter)

Species	Monodentate carbonate	Bidentate carbonate	Polydentate carbonate	Formyl
Schematic structure*	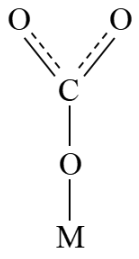	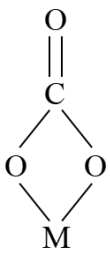	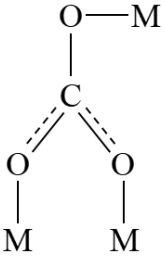	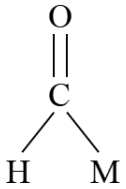

According to Figure 2.7, CO_2 forms various carbonate species. Subsequently, carbonates are hydrogenated by the surface hydrogen which is produced by either Ni and Ru: however, the role of Ru is more prominent than Ni, yielding 100% selectivity of CH_4 [1]. Moreover, formyl was identified with Ru(La-Ni)/Al_2O_3 which is fully absent without Ru [18]. Although detailed reaction kinetics is not fully identified by this DRIFTS analysis, the experimental observation agrees well with the reported methanation mechanisms [33]. The most important initial step of methanation is the formation of carbonates on metal-oxide support. Carbonates are further transformed into various intermediate species such as bicarbonate (HCO_3) and formate (HCOO). This reaction pathway is categorized as the "*CO_2 associative route*" where CO_2 is associatively adsorbed as carbonate and react with surface hydrogen to form carbonate/formate over the support materials. The support materials work as adsorption site for intermediate species until CH_4 is formed. Meantime, hydrogen molecules are dissociatively adsorbed on the metal surface that hydrogenates carbonate or formate consecutively towards CH_4. It should be emphasized that La, Ni, and Ru are well dispersed and overlapped in atomic scale as shown in HAADF-STEM imaging (Figure 2.1), indicating the interaction among surface species produced on both metal and support surfaces is efficient. Hydrogen spillover is strong on Ru which is essential for CH_4 formation, leading to 100% CH_4 selectivity. There is

a contribution of Ni for the surface hydrogen, however, the role on Ni is not as strong as Ru: CH_4 selectivity was limited to 60% at most with La-Ni/Al_2O_3 [1].

Regarding reaction enhancement by DBD, vibrationally excited CO_2 [34] would enhance CO_2 adsorption and carbonate formation which was proven in our previous study [18]. La provides active sites for anionic oxygen (O^{2-}) to react with adsorbed CO_2 [18]. In addition, La can further help adsorb CO_2 species, as well as increase the reducibility and basicity of Ni phase [35], which accelerates CO_2 conversion and explains the better performance on this catalyst. This reaction pathway is accelerated clearly by DBD. Another important reaction pathway is *"CO_2 dissociative route*" in which CO_2 is dissociatively adsorbed on metallic catalyst surface, creating adsorbed CO; CO is further hydrogenated into formyl [36], then CH_4 [2, 37, 38]. Although adsorbed CO was not identified in our study (around 2000-2100 cm^{-1}), formyl was formed only when Ru was add to the catalyst. With more surface hydrogen supply, CH_x is generated while oxygen is dissociated as either OH or O in the proximity to it [39-44]; adsorbed OH and O are key to promoting carbonate formation via *CO_2 associative route*. In Figure 2.7, neither formate nor CO was identified as intermediate species. Therefore, a detailed reaction pathway is hard to track from the DRIFTS observation. Meantime, carbonate formation was enhanced clearly by DBD which is a good correlation with enhanced CH_4 yield: therefore, CO_2 methanation occurs most likely via the associative route. In contrast, there is no remarkable change in the spectrum between Figure 2.7(b1) and (b2). Presumably, activation of H_2 by DBD has a small impact on the hydrogenation of carbonate species. In other words, hydrogen spillover would be sufficiently fast without DBD. Although peak intensity of p-carbonates and formyl increased by DBD to some extent, the role of those species in the formation of CH_4 under the presence of DBD is not clear yet.

2.7 Conclusion

DBD-assisted pulsed methanation was developed to suppress the rapid catalyst temperature increase due to the exothermic nature of the CO_2 methanation reaction.

As a result, the catalyst heating effect was minimized and the role of DBD was highlighted. Catalytic activity over two Ru based multi-metallic catalysts were studied. In comparison with Ni(Ru)/Al_2O_3, Ru(La-Ni)/Al_2O_3 exhibits a superior catalytic activity under the presence of DBD in terms of CO_2 and H_2 conversions at both 100 kPa and 30 kPa. The HAADF-STEM analysis of Ru(La-Ni)/Al_2O_3 supports that Ru, La, and Ni elements are well dispersed and overlapped in nanometer-scale which benefits interaction between surface species produced on each element. *In situ* DRIFTS study supports the possible reaction pathway of CO_2 methanation. La provides CO_2 adsorption sites and helps carbonate formation that is the key initiation step of methanation reaction. When DBD is applied, higher catalytic activities at low temperatures was confirmed because vibrationally excited CO_2 contributes formation of carbonate. Moreover, Ru promotes hydrogen spillover that hydrogenates CO_2-derived surface species. The combination of La and Ru is essential to promote the hybrid reaction with DBD.

2.8 Reference

1. Chen, X.; Sheng, Z.; Murata, S.; Zen, S.; Kim, H.-H.; Nozaki, T., CH_4 dry reforming in fluidized-bed plasma reactor enabling enhanced plasma-catalyst coupling. *Journal of CO_2 Utilization*, 2021, **54**, 101771.
2. Zhen, W.; Li, B.; Lu, G.; Ma, J., Enhancing catalytic activity and stability for CO_2 methanation on Ni-Ru/γ-Al_2O_3 via modulating impregnation sequence and controlling surface active species. *RSC Adv.*, 2014, **4**, 16472-16479.
3. Izumi, Y., Recent advances in the photocatalytic conversion of carbon dioxide to fuels with water and/or hydrogen using solar energy and beyond. *Coordination Chemistry Reviews*, 2013, **257**, 171-186.
4. Bogaerts, A.; Tu, X.; Whitehead, J. C.; Centi, G.; Lefferts, L.; Guaitella, O.; Azzolina-Jury, F.; Kim, H.-H.; Murphy, A. B.; Schneider, W. F.; Nozaki, T.; Hicks, J. C.; Rousseau, A.; Thevenet, F.; Khacef, A.; Carreon, M., The 2020 plasma catalysis roadmap. *Journal of Physics D: Applied Physics*, 2020**, 53**, 443001.
5. Albo, J.; Alvarez-Guerra, M.; Castaño, P.; Irabien, A., Towards the electrochemical conversion of carbon dioxide into methanol. *Green Chemistry*, 2015, **17**, 2304-2324.
6. Qiao, J.; Liu, Y.; Hong, F.; Zhang, J., A review of catalysts for the electroreduction of carbon dioxide to produce low-carbon fuels. *Chem Soc Rev*, 2014, **43**, 631-675.
7. Li, S.; Ongis, M.; Manzolini, G.; Gallucci, F., Non-thermal plasma-assisted capture and conversion of CO_2. *Chemical Engineering Journal*, 2021, **410**, 128335.
8. Wang, B.; Mikhail, M.; Cavadias, S.; Tatoulian, M.; Da Costa, P.; Ognier, S., Improvement of the activity of CO_2 methanation in a hybrid plasma-catalytic process in varying catalyst particle size or under pressure. *Journal of CO_2 Utilization*, 2021, **46**, 101471.
9. Kim, H.-H.; Abdelaziz, A. A.; Teramoto, Y.; Nozaki, T.; Hensel, K.; Mok, Y.-S.; Saud, S.; Nguyen, D. B.; Lee, D. H.; Kang, W. S., Interim report of plasma catalysis: Footprints in the past and blueprints for the future. *International Journal of Plasma Environmental Science and Technology*, 2021, **15**, e01004.
10. Snoeckx, R.; Bogaerts, A., Plasma technology - a novel solution for CO_2 conversion? *Chemical Society Reviews*, 2017, **46**, 5805-5863.
11. Dębek, R.; Azzolina-Jury, F.; Travert, A.; Maugé, F., A review on plasma-catalytic methanation of carbon dioxide - Looking for an efficient catalyst. *Renewable and Sustainable Energy Reviews*, 2019, **116**, 109427.
12. Yesgar, P. W.; Sheintuch, M., Nickel-catalyzed methanation reactions studied with an in situ magnetic induction method: Experiments and modeling. *Journal of*

Catalysis, 1991, **127**, 576-594.
13. Agnelli, M.; Kolb, M.; Mirodatos, C., CO Hydrogenation on a Nickel Catalyst .: 1. Kinetics and Modeling of a Low-Temperature Sintering Process. *Journal of Catalysis*, 1994, **148**, 9-21.
14. Ashcroft, A. T.; Cheetham, A. K.; Green, M. L. H.; Vernon, P. D. F., Partial oxidation of methane to synthesis gas using carbon dioxide. *Nature*, 1991, **352**, 225-226.
15. Jalama, K., Carbon dioxide hydrogenation over nickel-, ruthenium-, and copper-based catalysts: Review of kinetics and mechanism. *Catalysis Reviews*, 2017, **59**, 95-164.
16. Tsiotsias, A. I.; Charisiou, N. D.; Yentekakis, I. V.; Goula, M. A., Bimetallic Ni-Based Catalysts for CO_2 Methanation: A Review. *Nanomaterials*, 2021, **11**, 28.
17. Saeidi, S.; Najari, S.; Hessel, V.; Wilson, K.; Keil, F. J.; Concepción, P.; Suib, S. L.; Rodrigues, A. E., Recent advances in CO_2 hydrogenation to value-added products - Current challenges and future directions. *Progress in Energy and Combustion Science*, 2021, **85**, 100905.
18. Sheng, Z.; Kim, H. H.; Yao, S.; Nozaki, T., Plasma-chemical promotion of catalysis for CH_4 dry reforming: unveiling plasma-enabled reaction mechanisms. *Phys Chem Chem Phys*, 2020, **22**, 19349-19358.
19. Tou, A.; Kim, H.-H.; Einaga, H.; Teramoto, Y.; Ogata, A., Ozone-assisted catalysis of CO: In situ Fourier transform IR evidence of the cooperative effect of a bimetallic Ag-Pd catalyst. *Chemical Engineering Journal*, 2019, **355**, 380-389.
20. Kameshima, S.; Tamura, K.; Ishibashi, Y.; Nozaki, T., Pulsed dry methane reforming in plasma-enhanced catalytic reaction. *Catalysis Today*, 2015, **256**, 67-75.
21. Sheng, Z.; Sakata, K.; Watanabe, Y.; Kameshima, S.; Kim, H.-H.; Yao, S.; Nozaki, T., Factors determining synergism in plasma catalysis of biogas at reduced pressure. *Journal of Physics D: Applied Physics*, 2019, **52**, 414002.
22. Kim, D.-Y.; Ham, H.; Chen, X.; Liu, S.; Xu, H.; Lu, B.; Furukawa, S.; Kim, H.-H.; Takakusagi, S.; Sasaki, K.; Nozaki, T., Cooperative catalysis of vibrationally-excited CO_2 and alloy catalyst breaks the thermodynamic equilibrium limitation. *Journal of the American Chemical Society*, 2022, **144(31)**, 14140-14149.
23. Proaño, L.; Tello, E.; Arellano-Trevino, M. A.; Wang, S.; Farrauto, R. J.; Cobo, M., In-situ DRIFTS study of two-step CO_2 capture and catalytic methanation over Ru,"Na_2O"/Al_2O_3 Dual Functional Material. *Applied Surface Science*, 2019, **479**, 25-30.
24. Zheng, J.; Wang, C.; Chu, W.; Zhou, Y.; Köhler, K., CO_2 Methanation over Supported Ru/Al_2O_3 Catalysts: Mechanistic Studies by In situ Infrared

Spectroscopy. *ChemistrySelect*, 2016, **1**, 3197-3203.

25. Saito, A.; Sheng, Z.; Nozaki, T., In situ Raman spectroscopy of plasma-catalyst interface for conversion of CO_2 and CH_4 to valuable compounds. *International Journal of Plasma Environmental Science and Technology*, 2021**, 15**, e02007.
26. Jiao, X.; Li, L.; Zhao, N.; Xiao, F.; Wei, W., Synthesis and Low-Temperature CO_2 Capture Properties of a Novel Mg-Zr Solid Sorbent. *Energy & Fuels*, 2013, **27**, 5407-5415.
27. Yan, Y.; Dai, Y.; He, H.; Yu, Y.; Yang, Y., A novel W-doped Ni-Mg mixed oxide catalyst for CO_2 methanation. *Applied Catalysis B: Environmental*, 2016, **196**, 108-116.
28. Li, K.; Chang, X.; Pei, C.; Li, X.; Chen, S.; Zhang, X.; Assabumrungrat, S.; Zhao, Z.-J.; Zeng, L.; Gong, J., Ordered mesoporous Ni/La_2O_3 catalysts with interfacial synergism towards CO_2 activation in dry reforming of methane. *Applied Catalysis B: Environmental*, 2019, **259**, 118092.
29. Andriamasinoro, D.; Kieffer, R.; Kiennemann, A.; Rehspringer, J. L.; Poix, P.; Vallet, A.; Lavalley, J. C., Preparations and characterization of lanthana catalysts: study of their activity in CO/H_2 reactions. *Journal of Materials Science*, 1989, **24**, 1757-1766.
30. Shen, S. C.; Chen, X.; Kawi, S., CO_2 Adsorption over Si-MCM-41 Materials Having Basic Sites Created by Postmodification with La_2O_3. *Langmuir*, 2004, **20**, 9130-9137.
31. Kock, E. M.; Kogler, M.; Bielz, T.; Klotzer, B.; Penner, S., In Situ FT-IR Spectroscopic Study of CO_2 and CO Adsorption on Y_2O_3, ZrO_2, and Yttria-Stabilized ZrO_2. *J Phys Chem C Nanomater Interfaces*, 2013, **117**, 17666-17673.
32. Chen, H.; Goodarzi, F.; Mu, Y.; Chansai, S.; Mielby, J. J.; Mao, B.; Sooknoi, T.; Hardacre, C.; Kegnæs, S.; Fan, X., Effect of metal dispersion and support structure of Ni/silicalite-1 catalysts on non-thermal plasma (NTP) activated CO_2 hydrogenation. *Applied Catalysis B: Environmental*, 2020, **272**, 119013.
33. Mebrahtu, C.; Krebs, F.; Abate, S.; Perathoner, S.; Centi, G.; Palkovits, R., CO_2 Methanation: Principles and Challenges. In: Albonetti, S., Perathoner, S., Quadrelli, E.A., editors. *Horizons in Sustainable Industrial Chemistry and Catalysis*, Elsevier; 2019, pp. 85-103.
34. Adrianto, D.; Sheng, Z.; Nozaki, T., Mechanistic study on nonthermal plasma conversion of CO_2. *International Journal of Plasma Environmental Science and Technology*, 2020, **14**, e01003.
35. Wierzbicki, D.; Debek, R.; Motak, M.; Grzybek, T.; Gálvez, M. E.; Da Costa, P., Novel Ni-La-hydrotalcite derived catalysts for CO_2 methanation. *Catalysis Communications*, 2016, **83**, 5-8.

36. Saito, A.; Sheng, Z.; Kim, D.; Imamura, Y.; Nozaki, T., In situ transmission infrared spectroscopy of plasma-assisted CO_2 hydrogenation on ZnO: Role of catalyst support materials. *International Journal of Plasma Environmental Science and Technology*, 2021, ***15***, e02008.
37. Liu, Y.; Liang, X.; Zhang, J.; Yun, J.; Yang, Z., A low temperature organic synthesis of monodispersed NiRu nanocrystals for CO_2 methanation. *RSC Advances*, 2021, **11**, 2040-2046.
38. Vogt, C.; Monai, M.; Kramer, G. J.; Weckhuysen, B. M., The renaissance of the Sabatier reaction and its applications on Earth and in space. *Nature Catalysis*, 2019, **2**, 188-197.
39. Loveless, B. T.; Buda, C.; Neurock, M.; Iglesia, E., CO Chemisorption and Dissociation at High Coverages during CO Hydrogenation on Ru Catalysts. *Journal of the American Chemical Society*, 2013, **135**, 6107-6121.
40. Navarro-Jaén, S.; Szego, A.; Bobadilla, L. F.; Laguna, O.; Romero-Sarria, F.; Centeno, M.; Odriozola, J., Operando Spectroscopic Evidence of the Induced Effect of Residual Species in the Reaction Intermediates during CO_2 Hydrogenation over Ruthenium Nanoparticles. *ChemCatChem* 2019, **11**, 1-7.
41. Kattel, S.; Yan, B.; Chen, J. G.; Liu, P., CO_2 hydrogenation on Pt, Pt/SiO_2 and Pt/TiO_2: Importance of synergy between Pt and oxide support. *Journal of Catalysis*, 2016, **343**, 115-126.
42. Yang, Q.; Yin, X.; Wu, C.; Wu, S.; Guo, D., Thermogravimetric-Fourier transform infrared spectrometric analysis of CO_2 gasification of reed (Phragmites australis) kraft black liquor. *Bioresour Technol*, 2012, **107**, 512-516.
43. Yang, Q.; Wu, S.; Lou, R.; Lv, G., Structural characterization of lignin from wheat straw. *Wood Science and Technology*, 2011, **45**, 419-431.
44. Lochař, V., FT-IR study of methanol, formaldehyde and methyl formate adsorption on the surface of Mo/Sn oxide catalyst. *Applied Catalysis A: General*, 2006, **309**, 33-36.

Chapter 3: Auto-methanation with DBD treatment

3.1 Abstract

As CO_2 methanation is an exothermic reaction and nonthermal plasma (NTP) can provide both heat and synergy effect, CO_2 methanation under NTP treatment becomes possible. This chapter realized the above process on 4 types of catalysts including Ru-modified La-Ni/Al_2O_3, La-modified Ni/Al_2O_3, Ru/TiO_2 and Ru/Al_2O_3. As scaling up the reactor is another target in this chapter, 2 different diameter reactors were used (i.d. 20 mm & i.d. 30 mm). CO_2 conversion behaviors in a vertical packed-bed dielectric barrier discharge reactor at 80 kPa were investigated. Besides, whether self-sustained reaction is feasible or not after DBD-OFF was also observed. The low-temperature CO_2 methanation can be improved on Ru(La-Ni)/Al_2O_3 and La-Ni/Al_2O_3 by applying DBD to the reaction while DBD has no promotion effect on Ru/TiO_2 and Ru/Al_2O_3. With only DBD treatment, auto-methanation on all 4 catalysts becomes possible as DBD heating can help increase catalyst temperature to reaction temperature. However, self-sustained reaction only occurs on both monometallic Ruthenium catalysts due to their good catalytic activities around 200 °C.

3.2 Introduction

To accelerate low-temperature CO_2 conversion, nonthermal plasma (NTP) produced by dielectric barrier discharge (DBD) can be adopted because a part of CO_2 activation barrier can be removed under the impact between electron and excited CO_2 molecule activated by the plasma. It plays the similar role as it in the combustion process. When DBD is applied, it could efficiently produce methane even without external heating. This is one process intensification technique to improve the methanation process which usually requires heating at approximately 250-300 °C [1-3], which imparts a significant advantage to the process operation from an economic viewpoint. This also implies realization of auto-methanation becomes possible. Therefore, experiments are conducted to confirm the radical effect. Table 3.1 illustrates the experimental conditions in this chapter.

Table 3.1 Experimental conditions. Catalyst temperature: 100-400 °C; Pressure: 30/40 kPa & 80 kPa.

Catalyst	$Ru(La\text{-}Ni)/Al_2O_3$	$La\text{-}Ni/Al_2O_3$	Ru/TiO_2	Ru/Al_2O_3	Ru/Al_2O_3	Ru/Al_2O_3
Total flow rate (cm^3/min)	1200	1200	1200	1500	1500	5000
Catalyst weight (g)	13	13	13	25	29	29
WHSV ($cm^3/g/h$)	5538	5538	5538	3600	3103	10345
Power (W)	40	30	35	30	30	30
SEI (ev/molecule)	0.509	0.382	0.445	0.305	0.305	0.092
Frequency (kHz)	12	12	12	10	10	10
Thermal insulation	×	×	×	×	√	√
Reactor inner diameter (cm)	2	2	2	3	3	3

3.3 Experimental section

3.3.1 Experimental system

The experimental setup is shown in Figure 3.1. Most parts are the same as the ones indicated in chapter 2 except the reactor and power source. Two packed-bed dielectric barrier discharge (PB-DBD) reactors were employed in this chapter, the inner diameters of which are 20 mm and 30 mm respectively. They are both placed in the vertical direction. Inside the reactor four types of catalyst pallets were tested in sequence including Ru-modified La-Ni/Al_2O_3, La-modified Ni/Al_2O_3, Ru/TiO_2 and Ru/Al_2O_3. Prior to each experiment in which the type of catalyst is changed, the emissivity of new type of catalyst was quantified by calibrating the measured temperature data with thermocouples. This makes sure the gas temperature in the emission region matches up to the catalyst temperature. Gas flows downward through the high-voltage (HV) electrode inside hole so that gas can be preheated. As for power source, two kinds were used: one is 12 kHz-sinusoidal output (Logy Electric; LHV-13AC); the other is 10 kHz-asymmetrically peaked output (TAMAOKI ELECTRONICS CO.LTD; TE-HVP1510K300-NP).

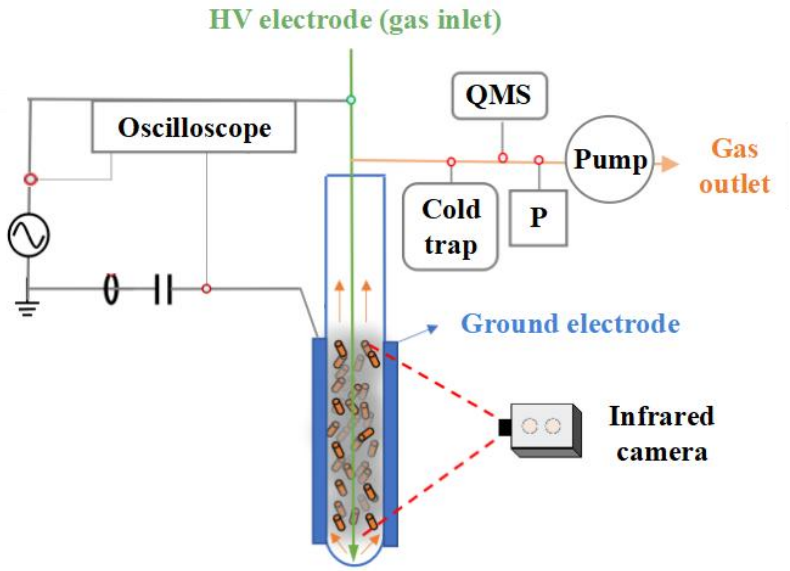

Figure 3.1 Experimental system of auto-methanation.

3.3.2 Temperature measurement

In auto-methanation reaction, because external heater is not necessary when DBD is applied to the reactor, the catalyst temperature profile can be obtained from the axial orientation as the ground electrode was designed in unclosed ring type as shown in Figure 3.1. However, to know the performance promotion by DBD, thermal catalysis experiment was also conducted in this chapter. For thermal catalysis using reactor with inner diameter of 20 mm, the reactor was fully wrapped by the external heater so that IR mirror was used to detect the catalyst temperature distribution at the bottom.

Catalyst temperature is determined by the heat balance. It includes heat generated by DBD (in plasma case) or the external heater (in thermal case), heat released from methanation reaction because of its exothermic character, and heat removed by heat conduction through reactor wall, heat convection through feed gas flow, and heat radiation of the catalysts. In this chapter, the highest catalyst temperature was regarded as the real-time reaction temperature. This can help with reaction monitoring to avoid excessive temperature increase that leads to catalyst deactivation or side reaction. On the other hand, it also becomes easier to know the temperature change during reaction process. However, one might think in the cases that only the bottom catalyst temperature distribution is obtained, it's hard to tell if the highest temperature at the bottom is the highest one in the whole reaction region. To understand this, the highest temperature confirmation experiment was conducted using the detachable heating device. A gap of 2 cm in width was left to facilitate the measurement of axial temperature distribution. The result proves that the highest catalyst temperature at the bottom is the highest temperature in the whole reaction region, which can be easily seen in Figure 3.2. The reason why temperature in non-catalyst region is high is this area is close to the center of heater so that the heat loss is less than that in area away from the heater center.

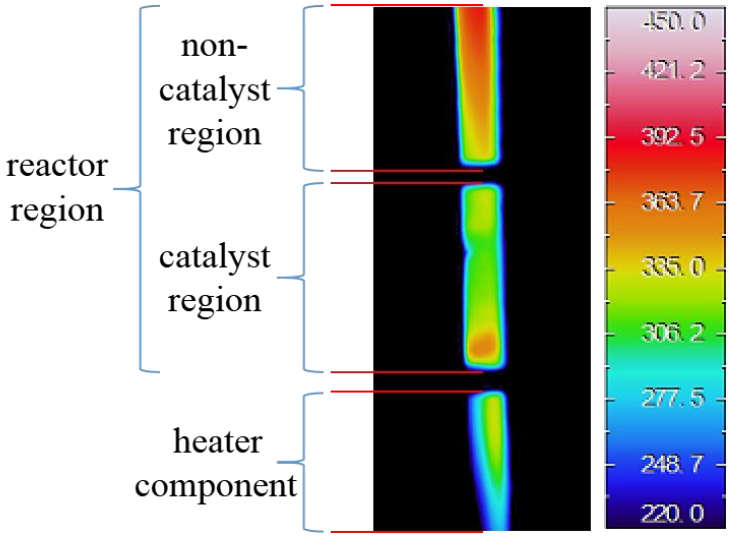

Figure 3.2 Image of axial temperature distribution in thermal catalysis.

3.4 Auto-methanation in PB-DBD reactor with inner diameter of 20 mm

In auto-methanation, 2 indicators are used to understand auto-methanation phenomenon, which include: (1) to see if reaction can be self-sustained after DBD-OFF; (2) to see time-dependent change in catalyst temperature.

3.4.1 Auto-methanation on Ru(La-Ni)/Al_2O_3

The time-dependent change in gas composition and catalyst temperature distribution is depicted in Figure 3.3. In thermal catalysis, after CO_2 conversion and catalyst temperature reached the maximum, the heater was turned off at 75 min. Without thermal insulation, the catalyst temperature gradually decreased and reaction finally stopped, which means self-sustain is unlikely on Ru(La-Ni)/Al_2O_3 in thermal case. The catalyst temperature distribution result indicates that although temperature difference of less than 50 °C exists, temperature distribution can be considered uniform. Then the temperature curve in Figure 3.3(a) can represent for the change in catalyst temperature distribution. In the following sessions, because the temperature distributions at the bottom in thermal catalysis are always uniform, these temperature figures are not shown in the paper.

For plasma catalysis, at the first 18 minutes, only H_2 (flow rate = 960 cm^3/min) was supplied to the PB-DBD reactor. Catalyst temperature increased to approximately

250 °C due to heat generation by DBD. CO_2 was not added to the system because it can be converted to CO with DBD treatment at temperature below 200 °C [4], which is not the main concerned product and may cause safety issue. As the measured temperature reached enough high for reaction, CO_2 (flow rate = 240 cm^3/min) was added to the system so that reaction occurred and catalyst temperature continued to increase due to DBD heating and DBD-promoted methanation. From 35 min to 45 min CO_2 conversion and catalyst temperature both achieved maximum and became stable, after which DBD was turned off so that heat generation by only thermal reaction was unable to compensate for the heat loss. As the catalyst temperature gradually decreased due to the stop of DBD and the weakening of methanation, reaction finally stopped after 50 min. It should be pointed out that the catalyst temperature at the reactor bottom was not always the highest reaction temperature in the whole experiment process. The axial temperature distribution was more uniform in H_2-DBD environment (15 min) and at the beginning when CO_2 was introduced (20 min). With the increase of catalyst temperature, the highest temperature began to appear in the lower part of the reactor rather than the bottom region (30 min). However, with further increase of catalyst temperature, the highest temperature eventually was concentrated at the bottom of the reactor (35 min and 40 min). The explanation to this is feed gas is preheated through heat transfer from the outside of electrode as it passes by the high-voltage electrode. If feed gas has already been preheated to an enough high temperature before it contacts with the catalyst, methanation reaction can rapidly happen and release a large quantity of heat when it contacts with the catalyst. So the highest temperature will finally move to the bottom of the reactor. The biggest difference in temperature distribution from top to bottom is about 150 °C, this is because at such experimental condition the net reaction time is large enough. Then most feed gas is converted at the lower part of reactor where most heat is generated while less heat is released from the upper reactor.

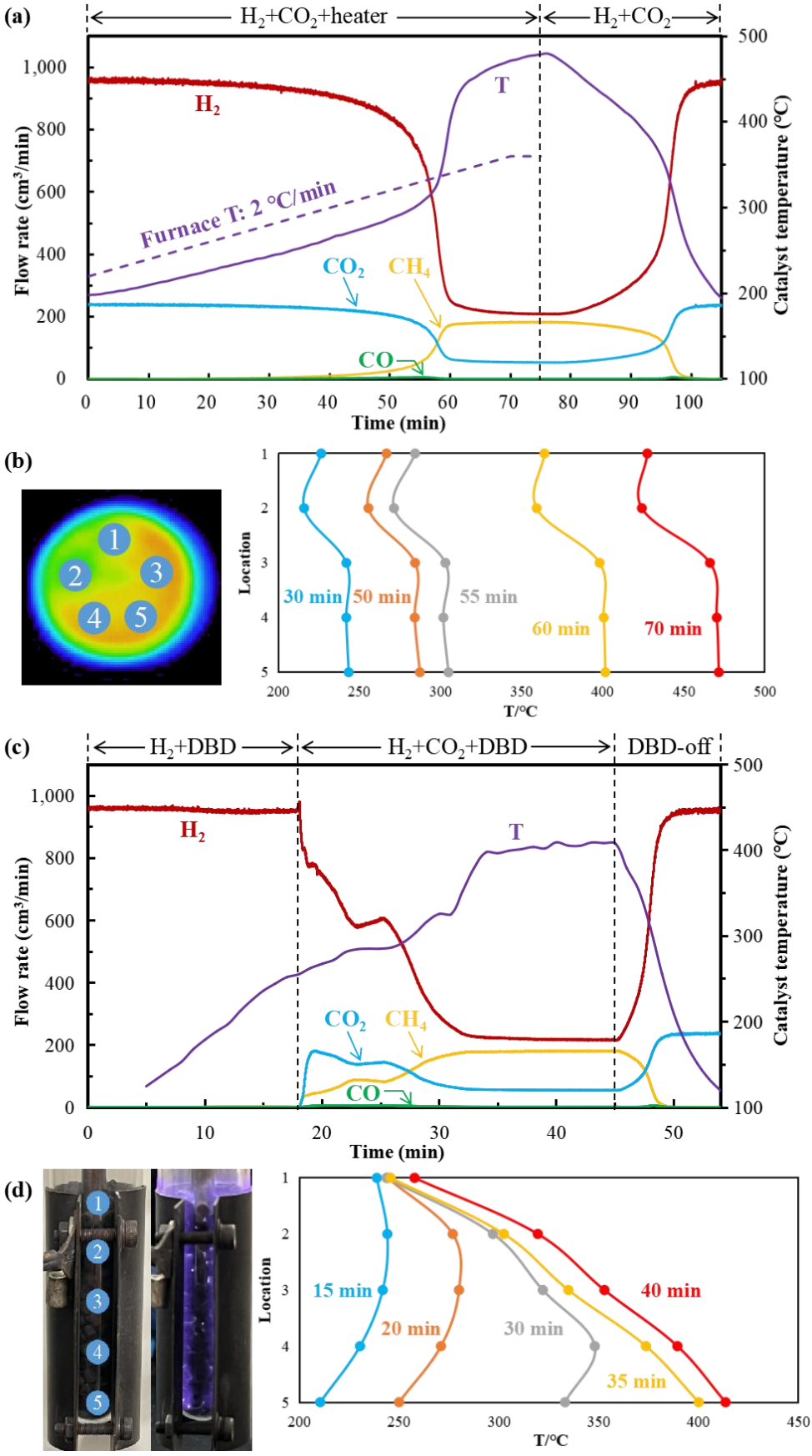

Figure 3.3 Time-dependent change in gas composition and catalyst temperature

distribution on Ru(La-Ni)/Al_2O_3: (a) gas composition in thermal catalysis; (b) temperature distribution in thermal catalysis; (c) gas composition in plasma catalysis; (d) temperature distribution in plasma catalysis.

Figure 3.4 shows CO_2 conversion behavior on Ru(La-Ni)/Al_2O_3 and compares it with thermodynamic equilibrium. The result indicates that CO_2 methanation is improved by DBD between 250 °C and 400 °C. As CO_2 conversions in both thermal and plasma catalysis are close to the equilibrium, the enhancement by DBD becomes less significant. It should be noted that in Chapter 2, CO_2 conversion achieves 75 % at 30 kPa on Ru(La-Ni)/Al_2O_3 which is close to the maximum of 77 % CO_2 conversion reaches at 80 kPa in vertical PB-DBD reactor case (Chapter 3). This is caused by different H_2/CO_2 ratios (in Chapter 2: 5:1; in Chapter 3: 4:1) while higher H_2/CO_2 ratio results in higher CO_2 conversion based on thermodynamic analysis. Another point is the performance promotion by DBD in vertical reactor is more significant than that in horizontal reactor. This can be explained by the fact that gas flow in horizontal direction results in higher turbulence and better mixing performance due to the lower pressure drop in horizontal reactors. Then uniform heat distribution inside the horizontal reactor becomes easier. The gas flow in vertical direction leads to poor mixing performance, which makes temperature different from the top to the bottom of the vertical reactor. The uniformity of temperature distribution affects the catalytic performance in these 2 types of reactors.

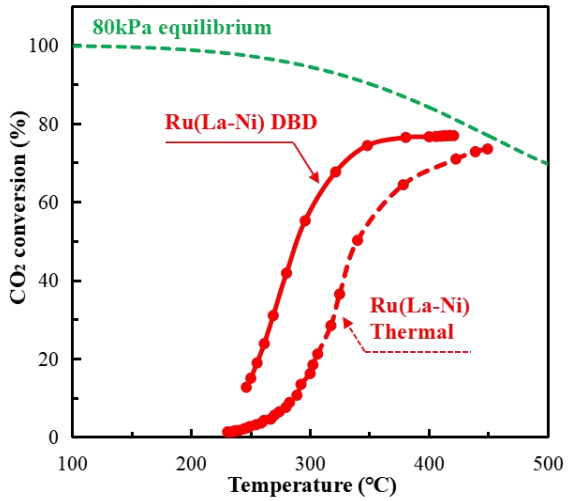

Figure 3.4 Catalytic activity on Ru(La-Ni)/Al_2O_3 at 80 kPa in vertical PB-DBD reactor.

3.4.2 Auto-methanation on La-Ni/Al_2O_3

Time-dependent change in gas composition and catalyst temperature distribution on La-Ni/Al_2O_3 is depicted in Figure 3.5. Self-sustain is unlikely to happen on La-Ni/Al_2O_3 in both thermal and plasma cases (data was not shown for thermal catalysis). In plasma catalysis, at the first 15 minutes, only H_2 (flow rate = 960 cm^3/min) was supplied to the PB-DBD reactor. As the catalyst temperature increased to approximately 250 °C, CO_2 (flow rate = 240 cm^3/min) was added to the system. At 45 min CO_2 conversion and catalyst temperature both achieved maximum and became stable, after which DBD was turned off. Because heat generation by only thermal reaction was unable to compensate for the heat loss, the catalyst temperature gradually decreased and reaction finally stopped after 55 min. From Figure 3.5(c), it can be seen that the highest temperature position change in the heating process (15 min, 35 min and 45 min) of La-Ni/Al_2O_3 is consistent with that of Ru(La-Ni)/Al_2O_3 while the highest temperature point is moved upward from the bottom in the cooling process (50 min and 55 min). It finally moves to the reactor center because heat loss in the center is the least.

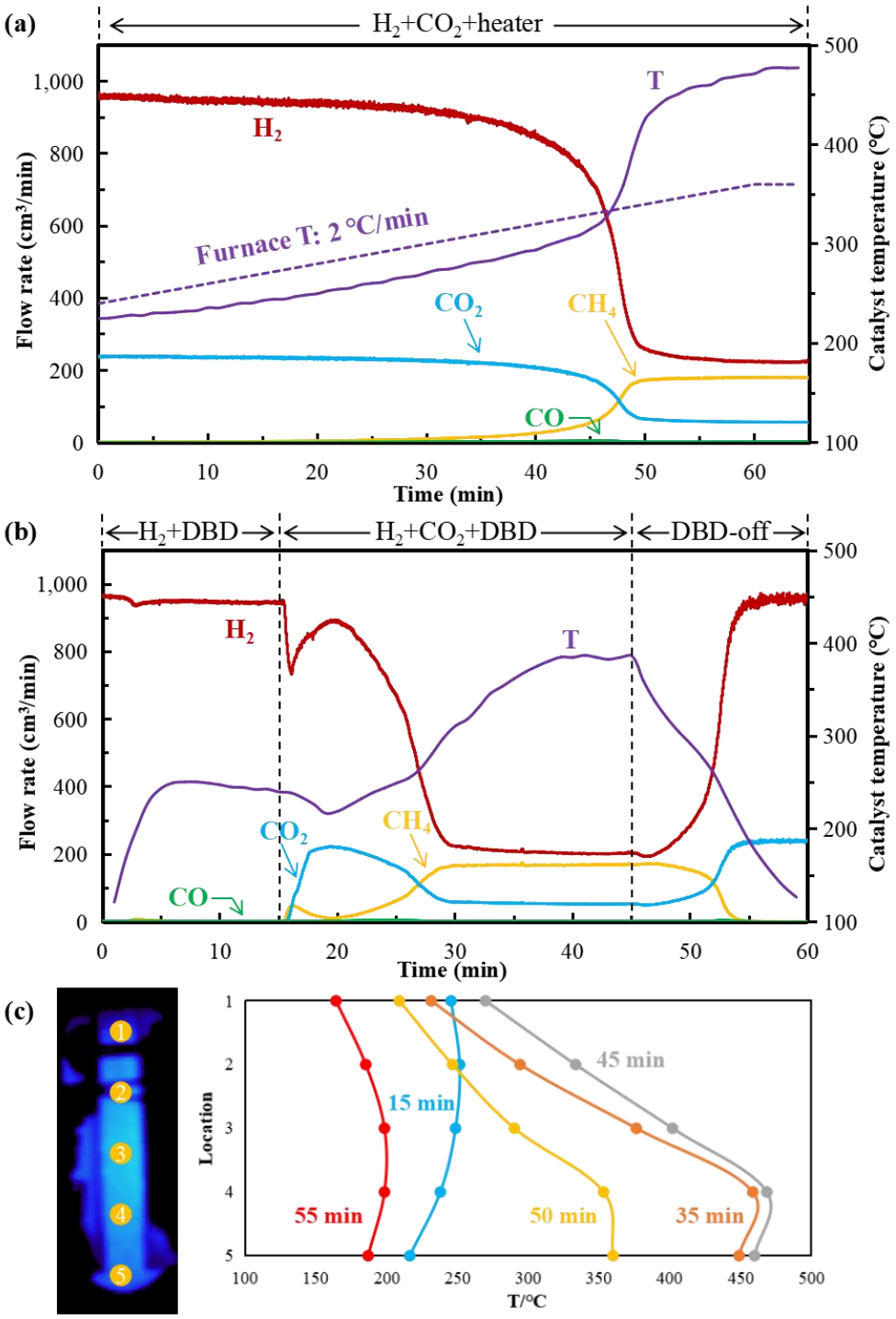

Figure 3.5 Time-dependent change in gas composition and catalyst temperature distribution on La-Ni/Al_2O_3: (a) gas composition in thermal catalysis; (b) gas composition in plasma catalysis; (c) temperature distribution in plasma catalysis.

Figure 3.6 compares CO_2 conversion behaviors on La-Ni/Al_2O_3 and Ru(La-Ni)/Al_2O_3. The result shows that the catalytic activities on both catalysts are quite the

same. CO_2 conversion promoted by DBD can be clearly seen between 250 °C and 400 ° C. As CO_2 conversions in both thermal and plasma catalysis are close to the equilibrium, the enhancement by DBD becomes less significant. The comparison result also indicates that Ru has little effect on promotion of catalytic performance. On the contrary, it emphasizes the significance of La in CO_2 methanation over La-contained catalysts.

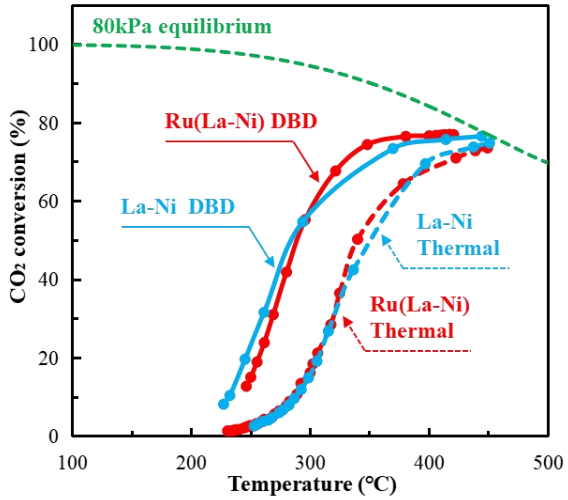

Figure 3.6 Comparison of catalytic activity on La-Ni/Al_2O_3 and Ru(La-Ni)/Al_2O_3 at 80 kPa in vertical PB-DBD reactor.

3.4.3 Auto-methanation on Ru/TiO_2

Time-dependent change in gas composition and catalyst temperature distribution on Ru/TiO_2 is depicted in Figure 3.7. It can be known that self-sustain becomes possible on Ru/TiO_2 in both thermal and plasma cases. In thermal catalysis, the heater was turned off at 40 min. And without thermal insulation, the catalyst temperature maintained so that reaction remained. For plasma catalysis, at the first 8 minutes, only H_2 (flow rate = 960 cm^3/min) was supplied to the PB-DBD reactor. As the catalyst temperature increased to about 150 °C, CO_2 (flow rate = 240 cm^3/min) was added to the system. It should be noted that the speed of catalyst temperature rise due to DBD heating is greater than that due to heating by traditional heaters. This can be seen by comparison between Figure 3.7(a) and Figure 3.7(b). At 30 min CO_2 conversion and

catalyst temperature both achieved maximum and became stable, after which DBD was turned off. Because heat generation by only thermal reaction gradually compensated for the heat loss, the catalyst temperature and reaction finally maintained after 55 min. In Figure 3.7(c), the highest temperature position change in the heating process (10 min, 20 min and 30 min) of Ru/TiO_2 complies well with that of $Ru(La-Ni)/Al_2O_3$. Although the catalyst temperature difference gets larger as DBD is turned off (40 min and 55 min), 80 % of CO_2 can still be converted thanks to the high conversion rate in the lower part of the reactor (This can be known from the catalytic activity result).

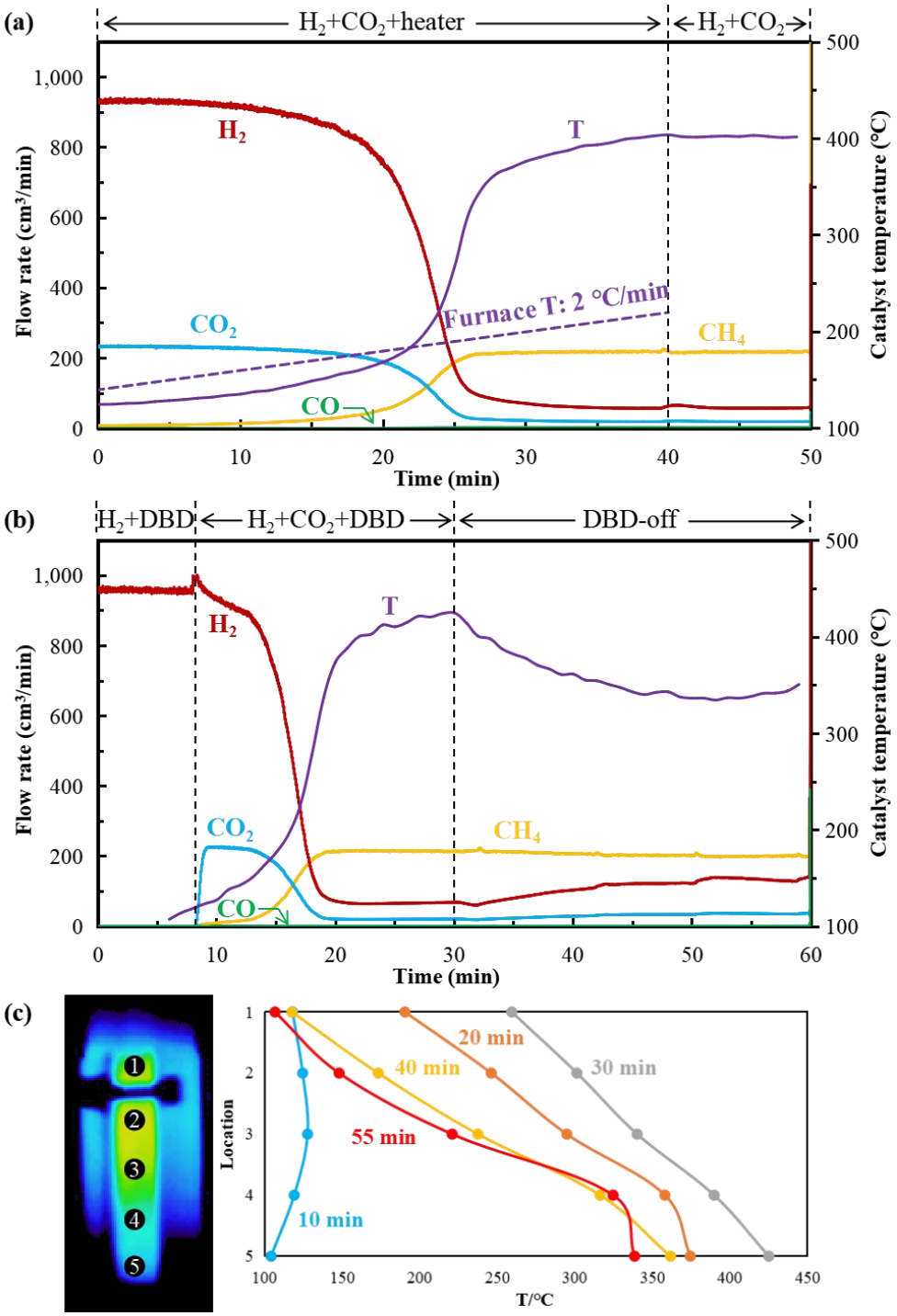

Figure 3.7 Time-dependent change in gas composition and catalyst temperature distribution on Ru/TiO_2: (a) gas composition in thermal catalysis; (b) gas composition in plasma catalysis; (c) temperature distribution in plasma catalysis.

Figure 3.8 compares CO_2 conversion behaviors on Ru/TiO_2 and $Ru(La\text{-}Ni)/Al_2O_3$. The result indicates DBD has no promotion on catalytic activity of Ru/TiO_2. However,

DBD still plays an important role as ignition. More importantly, the catalytic performance on Ru/TiO_2 is obviously better than that on $Ru(La\text{-}Ni)/Al_2O_3$. CO_2 conversion on Ru/TiO_2 achieves 50 % at 200 °C, at which temperature the reaction has not started on $Ru(La\text{-}Ni)/Al_2O_3$. Besides, the maximum conversion that can be reached on Ru/TiO_2 is about 90 %. These explain why 80% of CO_2 can still be converted in the whole catalyst region after DBD is turned off. Then the heat generation by these converted CO_2 is still enough to compensate for the heat loss from the reactor, making self-sustained reaction possible.

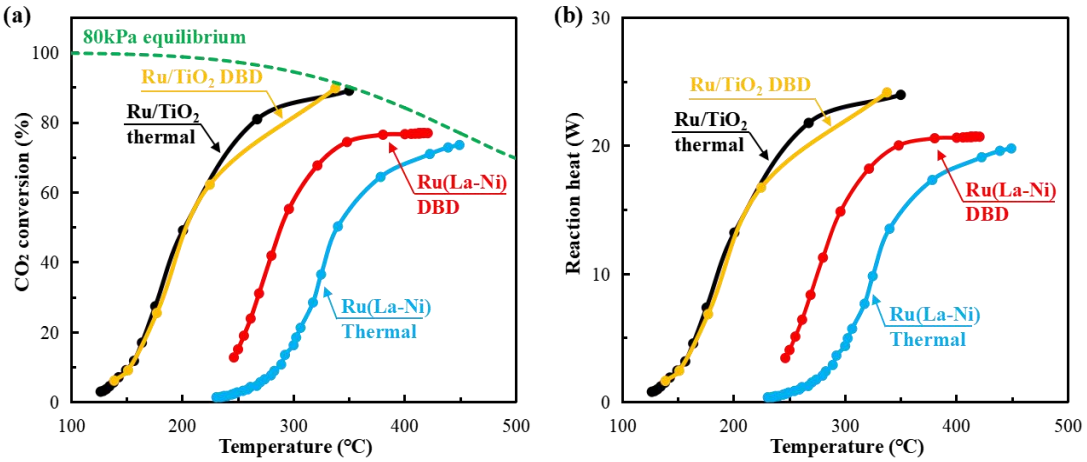

Figure 3.8 Comparison of catalytic activity on Ru/TiO_2 and $Ru(La\text{-}Ni)/Al_2O_3$ at 80 kPa in vertical PB-DBD reactor: (a) CO_2 conversion and (b) heat generated by methanation, respectively.

3.5 Auto-methanation in PB-DBD reactor with inner diameter of 30 mm

As scaling up the reactor under plasma-controlled thermal management is one of the targets in this chapter, PB-DBD reactor with inner diameter of 30 mm was studied.

3.5.1 Auto-methanation on Ru/Al_2O_3

As the inner diameter of the reactor has been enlarged, the heat loss increases accordingly which influences the heat balance and can fail to realize self-sustained reaction after DBD is turned off. To compensate for the heat loss, 2 types of methods

including generating more heat and preventing the heat loss, such as using thermal insulation, can be utilized. Considering these, in this section the total flow rate was increased from 1200 cm^3/min (in section 3.4) to 1500 cm^3/min and simultaneously the catalyst weight was added from 13 g (in section 3.4) to 25 g. These 2 measures would prolong the net reaction time and promote CO_2 conversion behaviors, further improving the heat generation. Besides, in this section Ru/Al_2O_3 was investigated instead of Ru/TiO_2 because TiO_2 is a semiconductor material. Electrical conductivity arises unexpectedly when electrons are transferred to their conduction band, which influences DBD generation in the reactor. And it has been proved the catalytic performance on Ru/Al_2O_3 is as good as that on Ru/TiO_2 and DBD can be well dispersed among Ru/Al_2O_3 catalysts, as shown in Figure 3.9.

Figure 3.9 DBD generated in vertical PB-DBD reactor (i.d.=30 mm) at 40 kPa with Ru/Al_2O_3 inside.

Time-dependent change in gas composition and catalyst temperature distribution on Ru/Al_2O_3 is depicted in Figure 3.10. In this and the following sessions, thermal catalysis experiment was not conducted because the similar catalytic activities on Ru/Al_2O_3 and Ru/TiO_2 are known and realization of auto-methanation with DBD treatment is the main target. In plasma catalysis, at the first 15 minutes, the gas pressure in the reactor was kept at 30 kPa because discharge at such pressure in a larger diameter reactor became easier. Only H_2 (flow rate = 1200 cm^3/min) was

supplied to the PB-DBD reactor. Same to Ru/TiO_2 case, as the catalyst temperature increased to about 150 °C, CO_2 (flow rate = 300 cm^3/min) was introduced to the system. When methanation was ignited and got stable, the gas pressure was increased to 80 kPa at 40 min so that heat generation was enhanced. As reaction got stable at 80 kPa, DBD was turned off at 60 min. However, as shown in Figure 3.10(a), the catalyst temperature gradually decreased and reaction finally stopped after 75 min because the heat loss was still too large in spite of more reaction heat generation. It is concluded that self-sustain is unlikely to happen under such conditions on Ru/Al_2O_3 in plasma catalysis. As for temperature distribution, the highest temperature position change in the heating process (20 min, 35 min and 50 min) and the cooling process (65 min and 70 min) of Ru/Al_2O_3 are in accordance with that of $Ru(La\text{-}Ni)/Al_2O_3$ and $La\text{-}Ni/Al_2O_3$, respectively. But unlike Ru/TiO_2 case, the highest temperature in Ru/Al_2O_3 case only achieves 350 ℃ (400 ℃ in Ru/TiO_2 case). This also implies the larger heat loss caused by larger reactor diameter, which also explains the rapid decrease in the highest temperature during DBD-OFF.

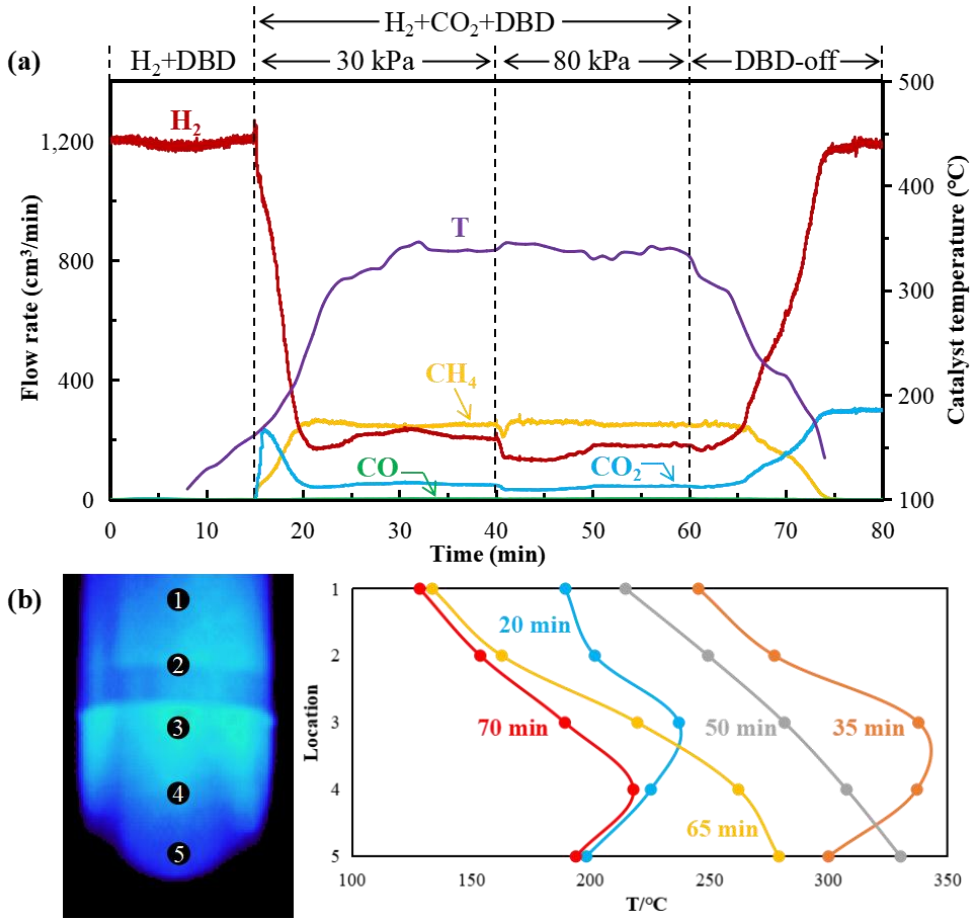

Figure 3.10 Time-dependent change in gas composition and catalyst temperature distribution on Ru/Al_2O_3: (a) gas composition in plasma catalysis; (b) temperature distribution in plasma catalysis.

Figure 3.11 illustrates CO_2 conversion behavior on Ru/Al_2O_3 and compares it with thermodynamic equilibrium. The result shows CO_2 conversions at both 30 kPa and 80 kPa achieve their maximum which are close to equilibrium. Because the net reaction time in this session is longer than that in Ru/TiO_2 case, CO_2 conversion reaches 60 % at 30 kPa and 200 °C on Ru/Al_2O_3, which is even 10 % higher than that at 80 kPa and 200 °C on Ru/TiO_2.

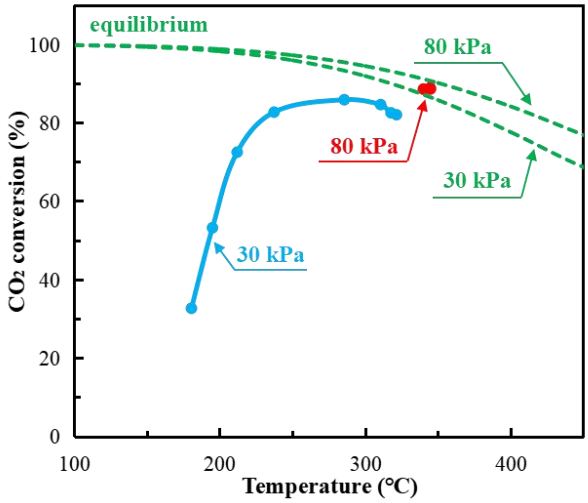

Figure 3.11 Catalytic activity on Ru/Al_2O_3 in vertical PB-DBD reactor.

3.5.2 Auto-methanation on Ru/Al_2O_3 with thermal insulation

Because the heat loss is too large for larger diameter reactor, as indicated in session 3.5.1, in this session the catalyst weight was increased to 29 g and a detachable heating device was used to provide thermal insulation, the temperature of which was set at 130 ℃. By doing so, more heat can be generated, but more importantly, the main cause of heat loss can be reduced. Besides, Ar was introduced to the reactor as dilution after DBD was turned off. This is because with thermal insulation self-sustained reaction becomes possible and the catalyst temperature eventually remains a certain value. As Ar was gradually added, the temperature and Ar flow rate at which reaction would stop were known. This helps provide information for scale-up design of the reactor.

Time-dependent change in gas composition and catalyst temperature distribution on Ru/Al_2O_3 with thermal insulation is depicted in Figure 3.12. In plasma catalysis, at the first 5 minutes, the gas pressure in the reactor was kept at 40 kPa. Only H_2 (flow rate = 1200 cm^3/min) was supplied to the PB-DBD reactor. CO_2 (flow rate = 300 cm^3/min) was then introduced as the catalyst temperature increased to about 150 °C. When methanation got stable, the gas pressure was increased to 80 kPa at 20 min. As reaction got stable at 80 kPa, DBD was turned off at 30 min. Then reaction maintained and the catalyst temperature remained at 310 ℃. So self-sustain has been

proved successful with thermal insulation. At 35 min, 1000 cm^3/min of Ar was introduced to the system, as the catalyst temperature gradually reduced, it finally remained at 265 °C. At 45 min, Ar flow rate was further increased to 2000 cm^3/min. Then reaction finally stopped after 70 min. As for temperature distribution, the highest temperature position change in the heating process (10 min and 25 min) and the cooling process (40 min, 55 min and 65 min) of Ru/Al_2O_3 with thermal insulation are consistent with that of $Ru(La\text{-}Ni)/Al_2O_3$ and $La\text{-}Ni/Al_2O_3$, respectively. After DBD was turned off, with the gradual dilution of Ar into the reactor, heat generated at the bottom was brought to the top of the reactor so that the highest temperature was moved to the top. Another reason for this is the top of the catalyst region was placed close to the heater center which has less heat loss.

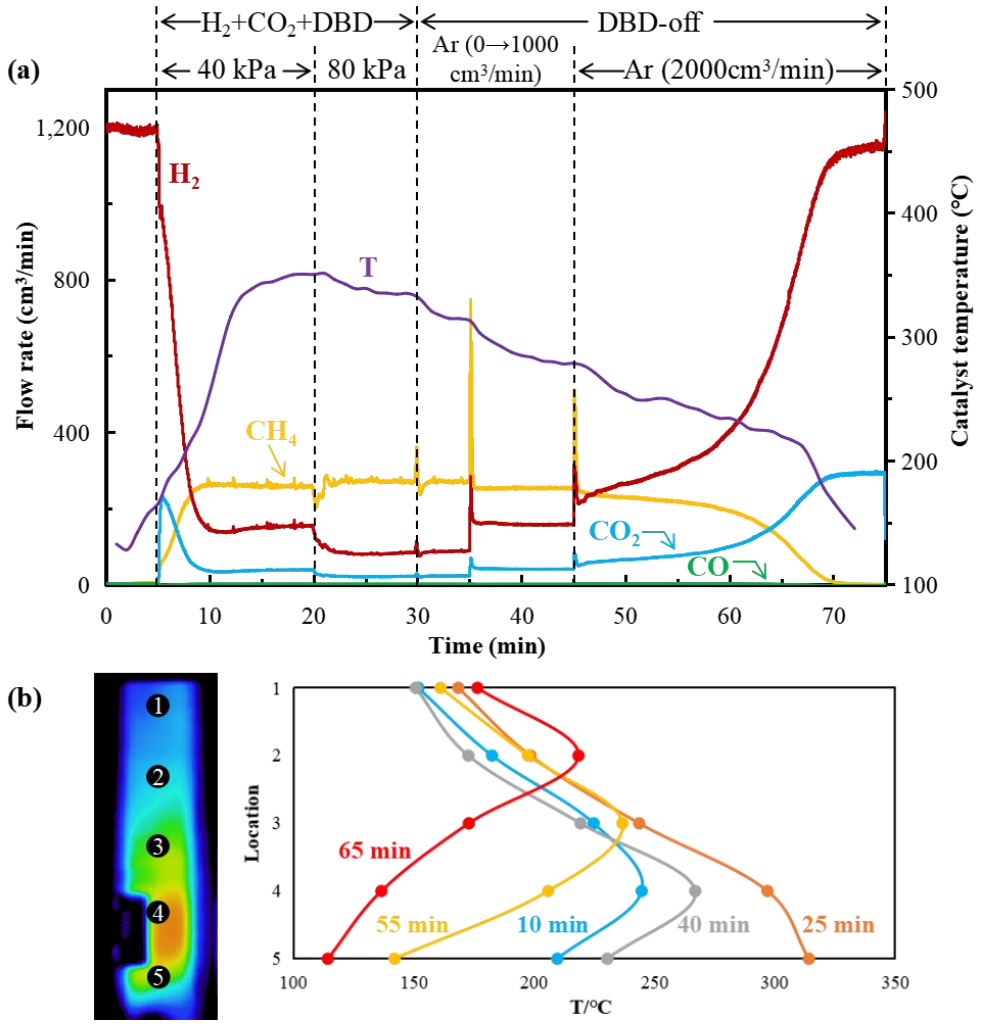

Figure 3.12 Time-dependent change in gas composition and catalyst temperature

distribution on Ru/Al_2O_3 with thermal insulation (furnace temperature: 130 °C, total flow rate: 1500 cm^3/min): (a) gas composition in plasma catalysis; (b) temperature distribution in plasma catalysis.

Figure 3.13 compares CO_2 conversion behaviors on Ru/Al_2O_3 with (40 kPa, 80 kPa) and without (30 kPa, 80 kPa) thermal insulation. The result shows that applying thermal insulation doesn't help with promotion of catalytic activity. The little higher CO_2 conversion for the case with thermal insulation at 80 kPa (curve in yellow) is mainly caused by the increase of net reaction time which is prolonged as the catalyst weight increases. The conversion difference between 40 kPa case and 30 kPa case is caused by not only net reaction time difference but also reaction pressure difference based on thermodynamic analysis.

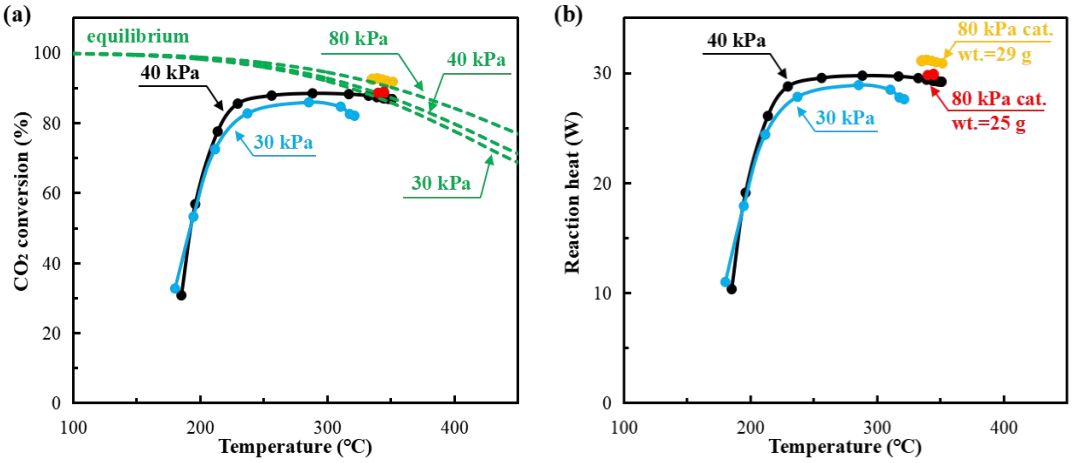

Figure 3.13 Comparison of catalytic activity on Ru/Al_2O_3 with and without thermal insulation in vertical PB-DBD reactor: (a) CO_2 conversion and (b) heat generated by methanation, respectively.

To further understand scale-up design of the reactor, a larger H_2/CO_2 flow rate of 5000 cm^3/min was supplied so that more heat would be generated. Then the Ar dilution to stop the reaction would also be changed. The time-dependent change in gas composition and catalyst temperature distribution under such condition is depicted in

Figure 3.14. In plasma catalysis, at the first minute, the gas pressure in the reactor was kept at 40 kPa. Only H_2 (flow rate = 4000 cm^3/min) was supplied to the PB-DBD reactor. As the catalyst temperature increased too fast, CO_2 (flow rate = 1000 cm^3/min) was introduced directly after 1 min. When methanation got stable, the gas pressure was increased to 80 kPa at 15 min. As reaction got stable at 80 kPa, DBD was turned off at 25 min. Then 4000 cm^3/min of Ar was introduced to the system, the catalyst temperature correspondingly reduced to 370 ℃. At 35 min, Ar flow rate was further increased to 5000 cm^3/min. Then reaction finally stopped after 45 min. As for temperature distribution, the highest temperature position change in the heating process (5 min, 10 min and 20 min) and the cooling process (30 min, 40 min and 45 min) of Ru/Al_2O_3 in larger flow rate complies with the law indicated in Figure 3.12.

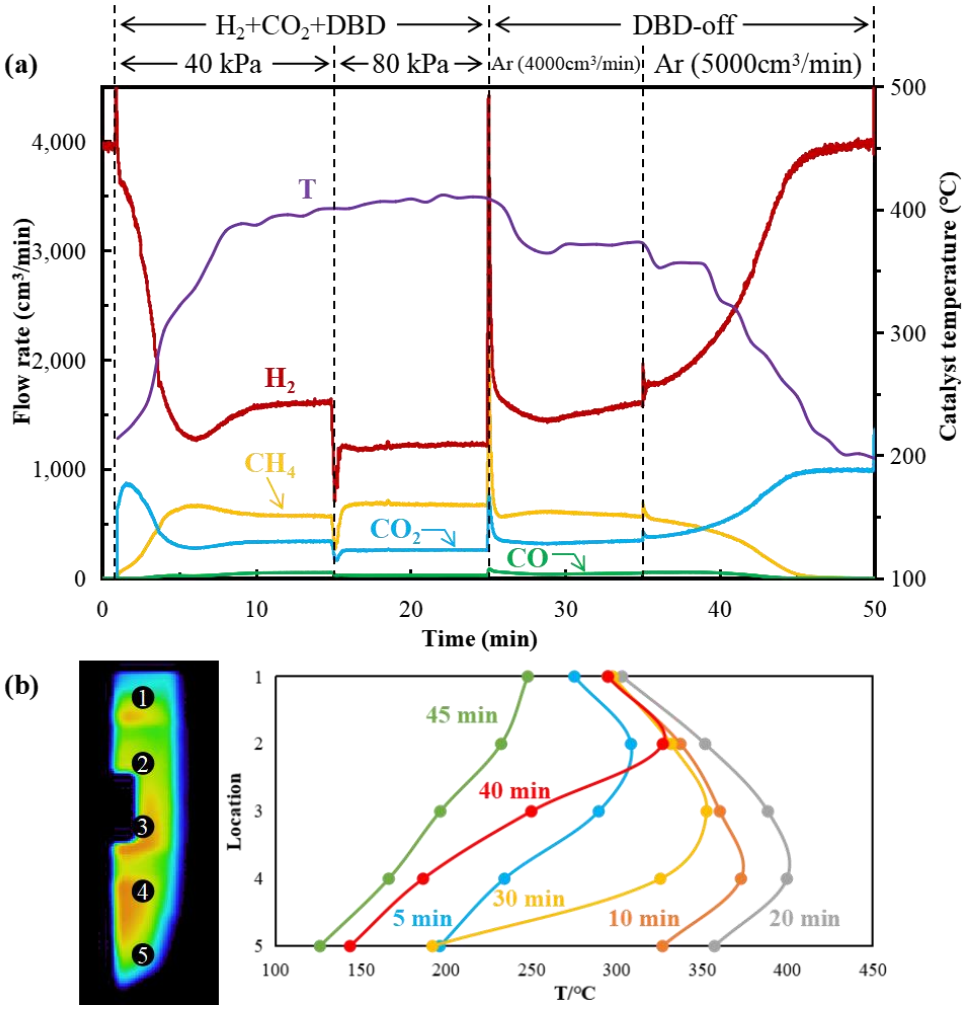

Figure 3.14 Time-dependent change in gas composition and catalyst temperature

distribution on Ru/Al_2O_3 with thermal insulation (furnace temperature: 130 °C, total flow rate: 5000 cm^3/min): (a) gas composition in plasma catalysis; (b) temperature distribution in plasma catalysis.

Figure 3.15 compares CO_2 conversion behaviors on Ru/Al_2O_3 in different flow rate conditions. The result shows that the catalytic activity at total flow rate of 5000 cm^3/min is lower than that at total flow rate of 1500 cm^3/min. This is because net reaction time is shortened as the total flow rate increases. However, despite a lower CO_2 conversion, as indicated in Figure 3.15(b), reaction heat achieves 80 W in larger flow rate, which is nearly 3 times higher than that in smaller flow rate case. With such big heat generation, it makes self-sustained reaction likely to be achieved after DBD is turned off. And it needs a larger amount of Ar diluted into the reactor so that the reaction can finally stop. In addition, from Figure 3.15(a), it can be seen CO_2 conversion is much lower than the equilibrium for larger flow rate case. This might be caused by the lower SEI, as shown in table 3.1.

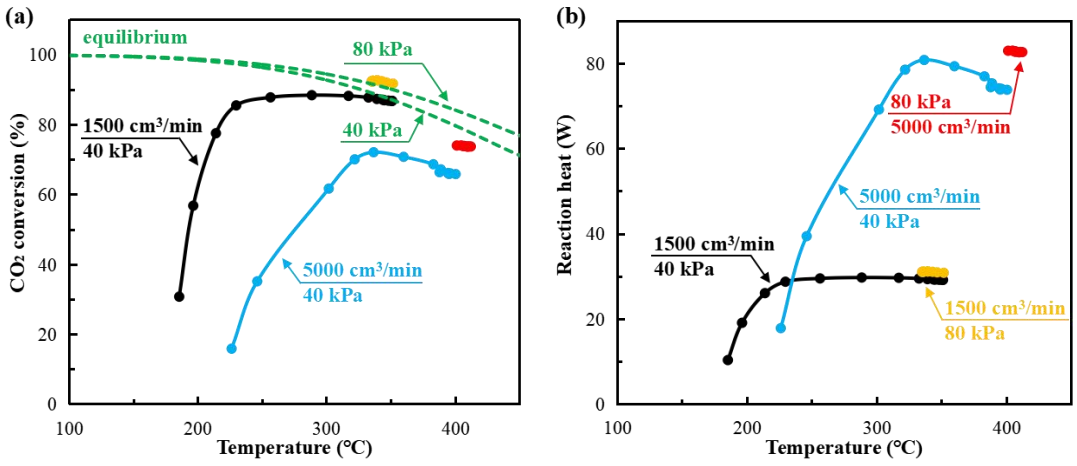

Figure 3.15 Comparison of catalytic activity on Ru/Al_2O_3 in different flow rate conditions in vertical PB-DBD reactor: (a) CO_2 conversion and (b) heat generated by methanation, respectively.

3.6 Conclusion

Auto-methanation can be achieved when enough discharge power is applied. DBD in this process plays important role as ignition (on Ru/TiO_2 & Ru/Al_2O_3) or even promotion (on $Ru(La\text{-}Ni)/Al_2O_3$ & $La\text{-}Ni/Al_2O_3$) if highly reactive species can well interact with catalyst surface. The monometallic Ruthenium catalysts prove potential catalysts to sustain methanation after DBD treatment. This is because high CO_2 conversion is still possible at low temperature region, promoting heat generation. However, long-term stability test on these catalysts is needed. It's worthwhile to find an appropriate catalyst whose activity can be well promoted by DBD. If so, DBD can be well used in auto-methanation with a lower power consumption. To scale up the reactor, the type of catalyst and prevention from heat loss are most significant factors. Catalyst that has good catalytic activity at such low temperature as 200 °C is preferred.

3.7 Reference

1 Fukuhara C, Ratchahat S, Suzuki Y, et al. Auto-Methanation of Carbon Dioxide: A Novel Route for Transforming CO_2 over Ni-Based Catalyst. *Chemistry Letters*. 2019, **48**: 196-199.

2 Fukuhara C, Kamiyama A, Itoh M, et al. Auto-Methanation for Transition-Metal Catalysts Loaded on Various Oxide Supports: A Novel Route for CO_2 Transformation at Room-Temperature and Atmospheric Pressure. *Chemical Engineering Science*. 2020, **219**.

3 Hirata N, Watanabe R, Fukuhara C. Performance Characteristics of Auto-Methanation Using Ru/CeO_2 Catalyst, Autonomously Proceeding at Room Temperature. *Fuel*. 2020, **282**.

4 Sun Y, Wu J, Wang Y, et al. Plasma-Catalytic CO_2 Hydrogenation over a Pd/ZnO Catalyst: In Situ Probing of Gas-Phase and Surface Reactions. *JACS Au*. 2022, **2**: 1800-1810.

Chapter 4: Conclusion

This thesis aims to demonstrate the feasibility of auto-methanation process on different types of catalysts. To this end, plasma-enhanced catalytic performance in the packed-bed dielectric barrier discharge reactor was confirmed at first (Chapter 2). *In situ* diffuse reflectance infrared Fourier-transform spectroscopy experiment was conducted to understand reaction mechanism (Chapter 2). Auto-methanation was designed when discharge power was sufficient for reactor to reach the initial reaction temperature (Chapter 3).

In Chapter 2, the low-temperature CO_2 methanation was improved by Ru-based multi-metallic catalyst and applying DBD to the reaction. Because La promotes adsorption of CO_2 via vibrational excitation. Besides, increasing the frequency from 12 kHz to 100 kHz at constant power can improve reaction performance because high-frequency operation enhances generation of vibrationally excited CO_2, further accelerating carbonate formation on catalysts. To better understand reaction mechanism in DBD environment, *in situ* diffuse reflectance infrared Fourier-transform spectroscopy (DRIFTS) was employed under the presence of DBD last year.

From *in situ* DRIFTS results, it was found that formation of carbonate species plays an important role in DBD-enhanced methanation reaction. Besides, the role of adding Ru and La into catalyst is also confirmed. It proves our catalyst can present a good catalytic performance and DBD environment can further promote it at a lower temperature. However, the role of formyl in the formation of CH_4 under the presence of DBD remains unclear. The reaction pathway is hard to track from the DRIFTS observation. So one plan for the future study is to figure out the reaction mechanism by means of Fourier-transform infrared spectroscopy (FTIR) analysis.

As nonthermal plasma is applied to promote catalytic performance, both heat and radicals generated by discharge are considered as impact factors. However, it is always hard to distinguish them. Thermodynamically, CO_2 methanation is an exothermic reaction, which is highly dependent on the temperature. The proper

management of exothermic energy generated during methanation is critical to developing the CO_2 conversion system on an industrial scale. To avoid thermal runaway from reactor, a better insulation system needs to be developed. Radicals promoting excited CO_2 generation has been reported in many methanation studies. It has great significance for achieving a higher CO_2 conversion with discharge at a much lower energy than reaction heat.

Methanation with nonthermal plasma treatment could efficiently produce methane even without external heating. This is one process intensification technique to improve the methanation process which usually requires heating at approximately 250-300 °C, which imparts a significant advantage to the process operation from an economic viewpoint. This also implies realization of auto-methanation becomes possible.

In Chapter 3, this study realized auto-methanation on 4 types of catalysts including Ru-modified La-Ni/Al_2O_3, La-modified Ni/Al_2O_3, Ru/TiO_2 and Ru/Al_2O_3. CO_2 conversion behaviors in a vertical packed-bed dielectric barrier discharge reactor at 80 kPa were investigated. Besides, whether self-sustained reaction is feasible or not after DBD-OFF was also observed. The low-temperature CO_2 methanation can be improved on Ru(La-Ni)/Al_2O_3 and La-Ni/Al_2O_3 by applying DBD to the reaction while DBD has no promotion effect on Ru/TiO_2 and Ru/Al_2O_3. With only DBD treatment, DBD heating can help increase catalyst temperature to reaction temperature. However, self-sustained reaction only occurs on both monometallic Ruthenium catalysts due to their good catalytic activities around 200 °C. DBD plays important roles as ‘ignition’ and ‘promotion’ once highly reactive species can well interact with catalyst surface. It should be pointed that long-term stability test on the catalyst is further needed.